Facies
DOI 10.1007/s10347-011-0290-0

ORIGINAL ARTICLE

# Facies and synsedimentary tectonics on a Badenian carbonate platform in the southern Vienna Basin (Austria, Central Paratethys)

**Thomas Wiedl · Mathias Harzhauser · Werner E. Piller**

Received: 7 July 2011 / Accepted: 13 December 2011


**Abstract** The Mannersdorf quarries at the northeastern edge of the Leitha Mountains (Lower Austria) preserve a record of pre-, syn- and post-tectonical phases of a Badenian carbonate platform in the Vienna Basin. The pre-tectonic phase is reported by a marine transgression with the development of a coastal slope scree and subsequent prograding of a Gilbert-type fan delta, overlain by very heterogeneous corallinacean limestones. A fault divides the study area into two independent tectonic blocks, which have been logged and subjected to detailed investigation and sampling. The corallinacean limestones of the first block indicate shallow-water environments (i.e., seagrass meadows) and gradual transitions from shallower to deeper environments, while the second block shows an unconformity, which is linked to a rapid facies change from relatively deeper environments (i.e., indicated by the abundance of in situ *Pholadomya*) to shallow waters (indicated by corals). Contrary to coral-bearing limestones of the same age at the southwestern part of the Leitha Mountains, corals are generally rare in the limestones of the Mannersdorf quarries, which represent mostly deeper environments with conspicuous differences in faunal associations. The onlap of limestones on a tectonic-caused flexure indicates syn-tectonical movements. Paleostress analyses verify a normal-fault reactivated as a dextral strike-slip fault. The temporal character of this fault is indicated by a post-tectonical phase with a marine transgression, a burial of the fault and neptunian dyke development.

**Keywords** Miocene · Langhian · Central Paratethys · Vienna Basin · Depositional environments · Synsedimentary tectonics · Facies

## Introduction

The Vienna Basin between the Eastern Alps and the Western Carpathians is one of the most studied basins—in terms of both structural and sedimentary geology (e.g., Royden 1985; Wessely 1988; Fodor 1995; Decker 1996; Strauss et al. 2006). The ca. 200 × 50 km large basin lies primarily within Austria, but extends into the Czech Republic and Slovakia (Wessely 2006). Its developmental history began with the formation of a pull-apart basin along the junction of the Eastern Alps and the Western Carpathians (Royden 1985). Interactive processes of compression, strike-slip movements and extension, related to compression and lateral extrusion led to its present-day appearance (Ratschbacher et al. 1991; Fodor 1995; Decker and Peresson 1996). The main extension activity occurred during the Middle Miocene, similar to the onset of extension in the Danube Basin (Ratschbacher et al. 1990). Basin subsidence led to fault tectonics at basin margins (Wessely 1983) and to synsedimentary filling of the newly formed accommodation space, especially during the Middle to Late Miocene (Wessely 2006). For this period, synsedimentary or buried faults are documented for the Vienna

T. Wiedl (✉) · W. E. Piller
Institute of Earth Sciences, Geology and Paleontology, University of Graz, Heinrichstrasse 26, 8010 Graz, Austria
e-mail: thomas.wiedl@uni-graz.at

W. E. Piller
e-mail: werner.piller@uni-graz.at

M. Harzhauser
Natural History Museum Vienna, Burgring 7, 1010 Vienna, Austria
e-mail: mathias.harzhauser@nhm-wien.ac.at

Published online: 18 January 2012

Basin (Seifert 1992; Fodor 1995). Subsidence rates often changed during basinal development and show intervals of increased rates especially during the Early Badenian (Lankreijer et al. 1995; Wagreich and Schmid 2002; Hohenegger and Wagreich 2011) with the highest rates of subsidence reaching 1,000 m/Ma in the south and around 700 m/Ma in the central part of the basin (Hölzel et al. 2008).

Throughout the Middle Miocene, the Vienna Basin was structured by several topographic highs that formed islands, shoals, and small platforms with extensive carbonate production (e.g., Dullo 1983; Riegl and Piller 2000; Schmid et al. 2001; Harzhauser and Piller 2010). One of these structures is represented by the Leitha Mountains in the southern part of the basin (Fig. 1). During the Middle Miocene the Leitha Mountains represented a shallow carbonate platform (Schmid et al. 2001). The basement is formed by pre-Cenozoic rocks, predominantly Central Alpine Crystalline units (Tollmann 1964) and Central Alpine Permian-Mesozoic units (Kröll and Wessely 1993) covered by Langhian and Serravallian limestones (corresponding with the Central Paratethyan Badenian and Sarmatian stages, see Fig. 1; Piller et al. 2007 for discussion) (Herrmann et al. 1993). Shallow-water carbonate rocks, widely known as Leitha Limestones (sensu Keferstein 1828), are widespread in the entire Central Paratethys during the Middle Miocene Badenian stage (Papp and Cicha 1978; Studencki 1988; Piller et al. 1991). The most dominant limestone constituents are coralline algae but locally corals formed small patch reefs and carpets (Riegl and Piller 2000). Within the Paratethyan realm during Miocene time the Vienna Basin was strongly influenced by the Alpine orogeny (Steininger and Rögl 1984). The Badenian, which was the acme of the Miocene carbonate production in the Central Paratethys (Harzhauser and Piller 2007), was also a time of increased tectonic activity in the Vienna Basin (Wessely 2006). Accordingly, synsedimentary tectonics were documented in lost quarries near Hof am Leithagebirge

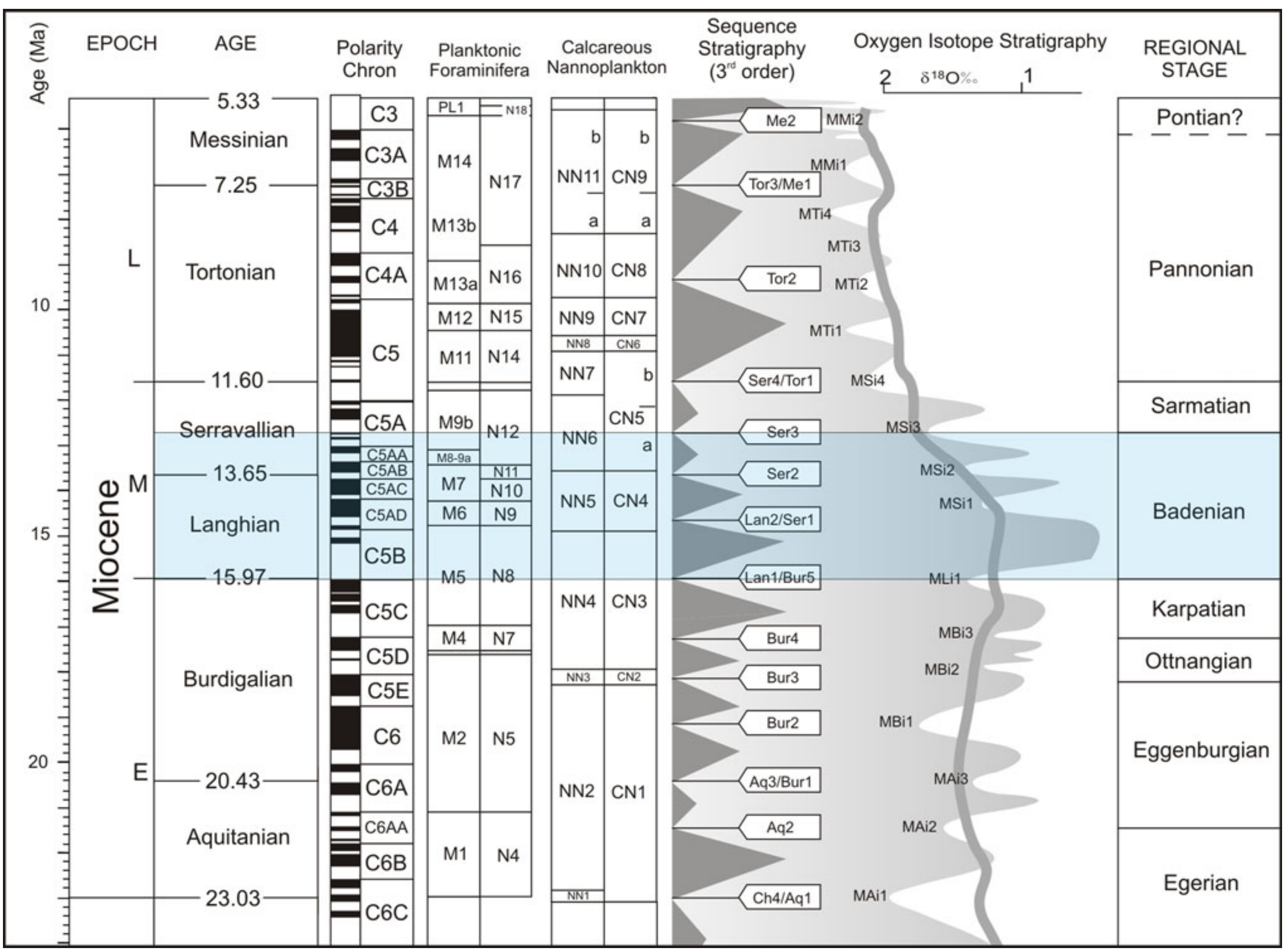


**Fig. 1** Stratigraphic table after Piller et al. (2007) including Miocene geochronology, geomagnetic polarity chrons, and biozonations of planktonic foraminifers and calcareous nannoplankton. Sequence stratigraphy and sea-level curve and oxygen isotope stratigraphy are correlated to regional chronostratigraphy of the Central Paratethys. The studied time interval (Badenian) is highlighted in *blue color*

(Schaffer 1908, Häusler et al. 2010). However, tectonic effects on the carbonate sedimentation regime in this area have not been documented.

In the present study, we describe an up to 80-m-thick carbonate succession from the largest active quarry in the Leitha Mountains at Mannersdorf (Lower Austria). The quarry is divided by a fault system into two tectonic blocks. Field observations and microfacies analyses demonstrate tectonically active and inactive phases as well as their influence on relative sea-level changes. The vertical and horizontal development of micro- and macrofacies within the succession also allows to interpret the temporal and spatial evolution of that part of the carbonate platform.

## Study area

The investigated outcrops are located within the active quarry system of the Lafarge-Perlmooser AG close to the village Mannersdorf in Lower Austria (Fig. 2). The geology of the Leitha Mountains close to Mannersdorf is characterized by an East Alpine basement, primarily composed of Middle Triassic dolostone and Semmering Quartzite, covered by Badenian Leitha Limestones

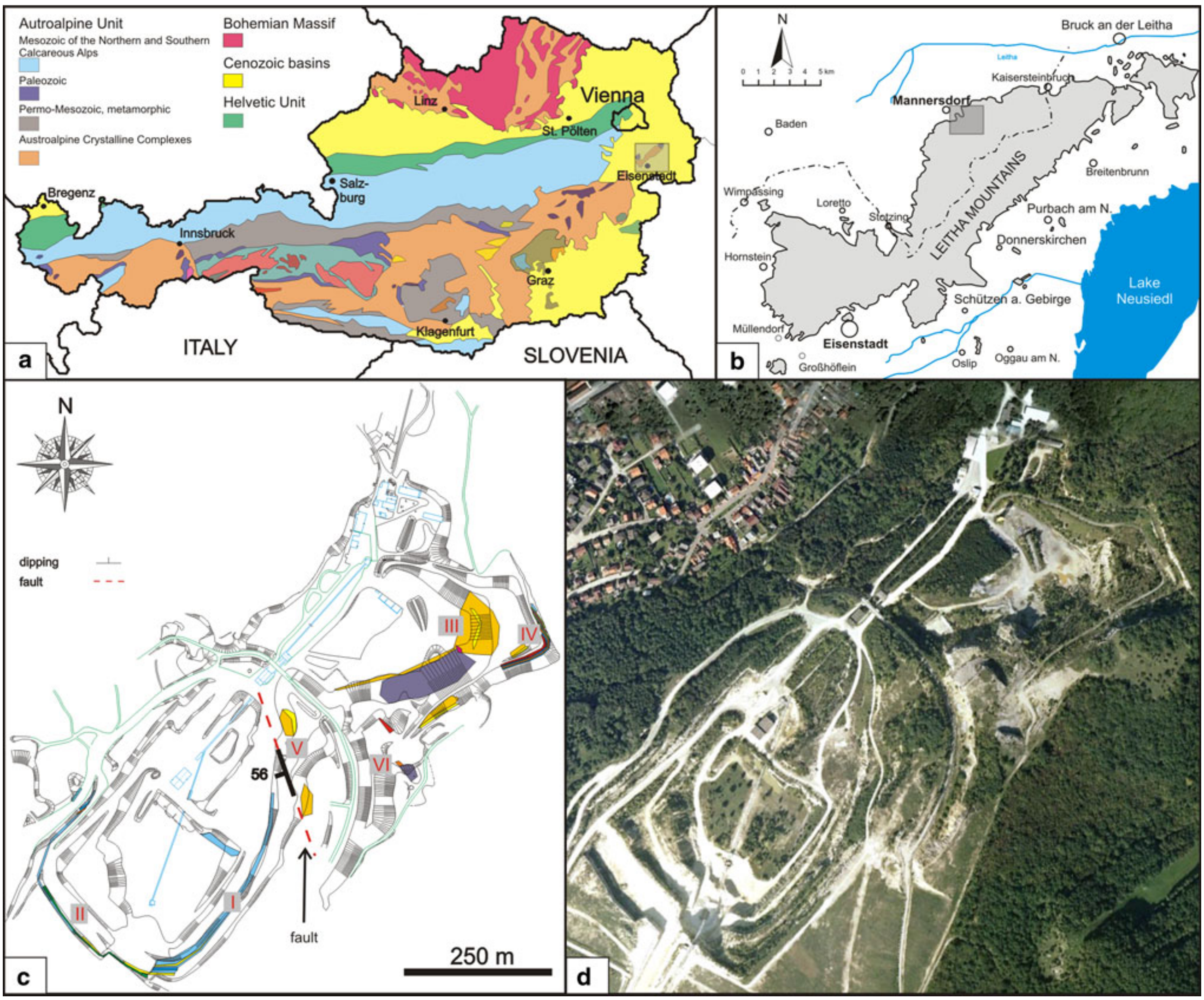


**Fig. 2** Location of the study area and indication of transects. **a** Geological map of Austria, simplified after Egger et al. (1999). **b** Geographic map (*inset* in **a**) of the Leitha Mountains spanning the border region of Lower Austria and Burgenland provinces. **c** Detailed map of *inset* in (**b**) of the Mannersdorf quarry system of Lafarge-Perlmooser AG (courtesy of Dipl.-Ing. Baehr-Mörsen) indicating the studied facies zonations (*colors* indicate facies types, cf. illustration in Fig. 3). *Roman numbers* indicate positions of the phototransects; fault dip is given by a symbol and a numerical value; the fault is marked by a *red line*. **d** Satellite image of the study area (**c**) 2011 Google corresponding to Fig. 1c

(Herrmann et al. 1993). The Mannersdorf quarries were only cursorily mentioned in the literature (Fuchs 1894; Schaffer 1908; Sohs 1963; Rohatsch 1997, 2008; Fencl 2005). Some of the described sections no longer exist due to intensive mining activity over many decades. A basic concept of the typical succession was proposed by Harzhauser and Piller (2004) for the nearby Baxa Quarry (ca. 1 km distance), which is characterized by Triassic dolostones overlain by Badenian and Sarmatian carbonates. Hydrothermal influence and hypogenic speleogenesis, which locally affects the Leitha Limestones, were described for a cave south of the Baxa Quarry (Plan et al. 2006).

## Materials and methods

Two sections, representative for the facies development of each tectonic block, have been logged and subjected to detailed investigation and sampling. The thickness of each bed was measured and oriented rock samples were collected for thin-section analyses. Due to the 3 to 10-m-high vertical walls, the reconstruction is based on a series of overlapping sub-sections (exact positions are indicated in Fig. 2). This enables the study of composite sections of almost 80 and 40 m thickness, respectively. For a detailed mapping of facies and faunal content and lateral facies-changes, photomosaics were prepared. For microfacies analyses, 47 thin-sections (5 × 5 cm) have been prepared. Carbonate nomenclature follows Dunham (1962) and Embry and Klovan (1971). The classification of siliciclastic sediments is based on terms of Wentworth (1922). Nomenclature of corallinacean growth forms follows Woelkerling et al. (1993). Field data of 26 slickensides and lineations were analyzed and plotted with Win-Tensor 3.0.0 of the TENSOR program (cf. Delvaux and Sperner 2003).

## Section description

Both sections are characterized by bedded limestones dominated by coralline algae debris. However, the corallinacean limestones differ in their faunal associations in each section. Additionally, the base of section II shows the transition from dolomitic basement to dolostone breccias and cross-bedded gravels overlain by corallinacean limestones. Skeletons with a primary calcite mineralogy, such as oysters, pectinids, and echinoids, are well preserved, while aragonitic biota are always dissolved or replaced by calcite. For example, corals occur as voids or sediment-filled corallites, while aragonitic bivalves are found as steinkerns or casts. Details (thickness, lithology, faunal content) of each bed, including results of thin-section analyses, are listed in Table 1.

### Section I

The succession starts with massive corallinacean limestones (bed 1 and 2) characterized by a macrofauna of various bivalves (oysters, pectinids, cardiids), gastropods (Conidae, Trochidae, *Cerithium*, *Xenophora*, *Turritella*) and rare echinoids. Toward the top of bed 1, a fining-upward trend is visible. The similar macrofauna of bed 2 (Fig. 4a) is additionally characterized by large *Gigantopecten nodosiformis* (de Serres in Pusch, 1837), *Glycymeris deshayesi* (Mayer, 1868) and *Thalassinoides* burrows. The transition between both beds (ca. 2 m) is not exposed. Ca. 100 m to the SSW, a lateral change within bed 2 from massive to a more porous marly limestone is visible and single in situ *Pinna tetragona* (Brocchi, 1814) occur in the upper part. There follows a massive corallinacean limestone (bed 3; Fig. 4b) which pinches out to the NNE that contains common molluscs as debris of oysters and pectinids or steinkerns of *Glycymeris deshayesi* and casts of *Periglypta miocaenica* (Michelotti, 1847). Articulated and disarticulated shells of *Gigantopecten nodosiformis* occur parallel to the bedding plane and form coquinas. Following the bed, ca. 130 m to the SW, it changes to a well-sorted corallinacean limestone. The marl content is variable and increases to the top of the bed where bioturbation is very common. Bivalve steinkerns are frequent; loosely dispersed *Gigantopecten nodosiformis* shells are intensely bored by sponges. Bed 4, which is onlapping on bed 3, starts with a distinct coquina of disarticulated shells of *Gigantopecten nodosiformis*. In the lower part, it is characterized by high marl content; the upper part gradually passes into a well-cemented limestone. Articulated *Glycymeris deshayesi* and *Periglypta miocaenica* are common throughout the bed. The following bed (5, Fig. 4c) is dominated by a soft, marly limestone with a macrofauna dominated by celleporiform bryozoans at the base, which occasionally encrust corallinaceans. Close to the boundary to bed 6, large and thick-branched rhodoliths (up to 7 cm in diameter) float within corallinacean debris. A 1-cm-thick intercalation of terrigenous silt (5a) separates bed 5 from the following bed (6), which contains common *Glans subrudista* (Friedberg, 1934), *Ctena decussata* (Costa, 1829), *Gigantopecten nodosiformis*, *Glycymeris deshayesi* and cardiids along with in situ *Pinna tetragona*. Fragments of branched *Porites* occur as well. Ca. 80 m to the W, small irregularly distributed quartz fine-sand lenses (up to ca. 0.5 m long and ca. 0.3 m thick) are intercalated within the bed. The bed is terminated by a 1 to 2-cm-thick silty clay bed, which is locally overlain by 1–3 cm of quartz fine-sand. The following bed (bed 7; Fig. 4c) is characterized by marly limestone containing many poorly preserved bivalves and gastropods (a few mm in size) and clusters of *Amphistegina* mass occurrences are typical.

**Table 1** Thickness, lithology, microfacies, and faunal content of each bed

| Section | Bed | Thickness | Lithology | Fossil content |
|---|---|---|---|---|
| I | 1 | 6.2 m | Massive corallinacean rudstone with packstone matrix or locally diffuse packstone areas dominated by debris (∅ 2–5 mm) of fruticose (c) and encrusting corallinaceans (r) growth forms; nodular rhodoliths (∅ 3 cm, r) | Bivalves: cardiids (c), ostreids (c), pectinids (c); gastropods: Conidae (r), Trochidae (r), *Cerithium* (c), *Xenophora* (r), *Turritella* (c); echinoids: cidariids (r), *Clypeaster* (r); celleporiform bryozoans (r, <5 mm); *Thalassinoides* (∅ 1–2 cm, c); foraminifers: *Amphistegina* (r), textulariids (r) |
| | 2 | 11 m | Massive, poorly sorted corallinacean rudstone with packstone matrix dominated by debris (∅ 2–5 mm) of fruticose (c) and thin encrusting growth forms (r); nodular rhodoliths (∅ 3 cm, s); *Acervulina* (r) | Bivalves: *Gigantopecten nodosiformis* (c), *Glycymeris deshayesi* (c), *Pinna tetragona* (s); gastropods: Conidae (c), rissoids (m), trochids (c); celleporiform bryozoans (<5 mm, r); echinoids: *Clypeaster* (r), disarticulated cidariids (c); foraminifers: *Planostegina* (r), *Amphistegina* (r), textulariids (r); *Thalassinoides* (∅ 1–2 cm, c) |
| | 3 | 2.15 m | Massive corallinacean rudstone with packstone matrix dominated by debris (∅ 4–5 mm) of fruticose (c) and encrusting (r) growth forms; *Acervulina*-corallinacean macroids (∅ 2–3 cm, c); spheroidal to ellipsoidal rhodoliths (∅ 5–7 cm, r) | Bivalves: *Gigantopecten nodosiformis* (m), *Glycymeris deshayesi* (c), *Periglypta miocaenica* (c), pycnodont oysters (r); gastropod steinkerns (<5 mm, r); branched and celleporiform (∅ 3–4 cm, r) bryozoans; foraminifers: *Amphistegina* (c), biserial textulariids (r), miliolids (r), globigerinids (s) |
| | 4 | 8.1 m | Corallinacean rudstone with packstone matrix dominated by debris (∅ 2–3 mm) of fruticose growth forms | Bivalves: *Gigantopecten nodosiformis* (c), ostreids (c), *Glycymeris deshayesi* (c), *Periglypta miocaenica* (c); echinoid spines (c); foraminifers: *Elphidium* (c), *Amphistegina* (r), textulariids (r) |
| | 5 | 6.7 m | Soft, marly corallinacean rudstone to floatstone with packstone matrix dominated by debris (∅ 4 mm) of fruticose (c) and thin encrusting (r) growth forms; locally rhodoliths (∅ 7 cm, c) | Bivalves: shell fragments (<3 mm, c); serpulids (r); locally celleporiform bryozoans (∅ 1–2 cm, c); foraminifers: *Amphistegina* (c), biserial textulariids (r), miliolids (*Triloculina*, r), globigerinids (s); rare and poorly preserved nannoplankton: *Coccolithus pelagicus* (Wallich, 1877) Schiller 1930, *Coronocyclus nitescens* (Kamptner, 1963, Bramlette and Wilcoxon, 1967) |
| | 5a | 1 cm | Dark silty clay | – |
| | 6 | 1.7 m | Corallinacean rudstone with packstone to wackestone matrix dominated by debris (∅ 2–5 mm) of fruticose (c) and thin encrusting (c) growth forms; locally fine-quartz-sand lenses (0.5 × 0.3 m) | Bivalves: *Glans subrudista* (c), *Ctena decussata* (c), *Gigantopecten nodosiformis* (c), *Glycymeris deshayesi* (c), cardiids (c), *Pinna tetragona* (m); coral: *Porites* (m); foraminifers: *Amphistegina* (c), biserial textulariids (c), miliolids (s) |
| | 6a | 1–2 cm | Dark silty clay | – |
| | 7 | 5.1 m | Marly corallinacean rudstone with wackestone matrix dominated by debris (∅ 2–4 mm) of thin encrusting (c) and fruticose growth forms (c); spheroidal to ellipsoidal rhodoliths (ca. 5 cm, s) | Bivalves: shell fragments (<3 mm, c), *Pinna tetragona* (m), *Gigantopecten nodosiformis* (c), *Aequipecten malvinae* (r), *Ctena decussata* (c), *Codakia* (c); gastropods: steinkerns (<5 mm, c); celleporiform bryozoans (∅ 1–2 cm, r); foraminifers: *Amphistegina* (m), biserial textulariids (r), miliolids (s), globigerinids (r); *Thalassinoides* (∅ 1–2 cm, c) |
| | 7a | 0.3–0.5 cm | Dark silty clay | – |
| | 8 | 28 cm | Well-cemented corallinacean rudstones with packstone matrix dominated by debris (ca. 400–700 μm thick) of thin encrusting (c) and rare fruticose (r) growth forms | Bivalve: *Pinna tetragona* (r); foraminifer: *Amphistegina* (c); echinoid debris and spines (r); serpulids (r); *Thalassinoides* (∅ 1–2 cm, c); celleporiform bryozoans (r) |
| | 8a | 0.5 cm | Dark silty clay | – |
| | 9 | 1.4 m | Corallinacean rudstone with packstone matrix dominated by debris (∅ 1–2 mm) of thin encrusting (c) and fruticose (r) growth forms | Bivalves: *Pinna tetragona* (m), cardiids (c), *Gigantopecten nodosiformis* (c); celleporiform bryozoans (r); *Thalassinoides* (∅ 1–2 cm, c) |

**Table 1** continued

| Section | Bed | Thickness | Lithology | Fossil content |
|---|---|---|---|---|
| | 9a | 1 cm | Dark silty clay | – |
| | 10 | 7.5 m | Massive corallinacean rudstone to floatstones dominated by debris (∅ 2–3 mm) of fruticose (c) and encrusting (r) growth forms | Bivalves: *Periglypta miocaenica* (c), *Glycymeris deshayesi* (c), *Pinna tetragona* (c); celleporiform bryozoans (r); echinoid debris (r); fish: spariid teeth (r); foraminifers: *Amphistegina* (r), textulariids (r), miliolids (s) |
| | 11 | 4.1 m | Well-sorted, poorly cemented soft chalky corallinacean rudstone of debris (∅ 5 mm) with packstone matrix consisting of fragments (∅ 1–2 mm) of fruticose (c) and thin encrusting (r) growth forms | Bivalves: *Gigantopecten nodosiformis* (c), *Glycymeris deshayesi* (c); gastropods: *Turritella* (r), Conidae (c); foraminifer: *Amphistegina* (r) |
| | 12 | 5.5 m | Corallinacean rudstones to floatstones with packstone matrix dominated by debris (∅ 1–4 mm) of thin encrusting growth forms | Bivalves: *Glycymeris deshayesi* (c), *Pinna tetragona* (r), *Gigantopecten nodosiformis* (c); bryozoans: branching (r); foraminifers: *Amphistegina* (r), textulariids (r) |
| | 13 | 11.5 m | Corallinacean rudstones to packstones dominated by debris (∅ 1–4 mm) of thin encrusting (c) and fruticose (c) growth forms; 500 m to the ENE: poorly cemented corallinacean rudstones dominated by debris (∅ 2–6 mm) of encrusting (c) and fruticose (r) growth forms; *Acervulina* (r) | Gastropods: *Cerithiopsis* (c), *Trochus* (c); bivalves: *Gigantopecten nodosiformis* (c), *Spondylus* (s); echinoid: *Arabacina* cf. *macrophyma* (c); serpulids (c); bryozoans: celleporiform (∅ 3 cm, c), branched (c); foraminifers: *Amphistegina* (m), *Planostegina* (r), textulariids (c), miliolids (r); *Thalassinoides* (∅ 1–2 cm, c) |
| | 14 | 4.4 m | Light massive corallinacean rudstone with wacke—to grainstone matrix dominated by debris (∅ 0.5–2 mm) of fruticose (c) and thin encrusting (r) growth forms | Bivalve: *Gigantopecten nodosiformis* (c); bryozoans (r); echinoid debris (r); foraminifers: *Amphistegina* (r), textulariids (r), miliolids (r) |
| II | 0 | ca. 30 m | Dark-grey massive dolostone | – |
| | 1 | 1.5 m | White silt | – |
| | 2 | 0.5 m | Monomictic dolostone breccia of subangular components (up to 20 cm diameter) and silty sand | – |
| | 3 | 0.6 m | Monomictic dolostone breccia of subangular components (5–7 cm) and silty sand | – |
| | 4 | 1.1 m | Monomictic dolostone breccia of subangular components (1–5 cm) and silty sand | Entobia (r) |
| | 5 | ca. 15 m | Non-cemented, well-rounded but poorly sorted gravel consisting of granite-, quartz- and dolostone-pebbles with alternating coarse (grain size: 5–7 cm) and fine layers (grain size: 1–2 cm) containing quartz-fine-sand | – |
| | 6 | 0.1–0.15 m | Calcareous quartz-fine-sandstone | – |
| | 7 | 0.6–0.8 m | Marly corallinacean rudstone with packstone matrix dominated by debris (∅ 4–5 mm) of laminar (c) and fruticose (r) growth forms; well-rounded quartz components (∅ 1–1.5 cm, c); rhodoliths (∅ 2–3 cm, r) and *Acervulina*-corallinacean macroids (∅ 3–4 cm, r) | Echinoids: debris (c) |
| | 8 | 7 m | Non-cemented, well-rounded but poorly sorted gravel consisting of granite-, quartz- and dolostone-pebbles (∅ 1–7 cm) and quartz-fine-sand (up to 50 in amount) | – |
| | 9 | 0.4–0.6 m | Quartz-fine-sand | – |
| | C1 | 1.5 m | Corallinacean rudstones to floatstones with mud- to wackestone matrix dominated by debris (∅ 4–6 mm) of encrusting corallinaceans (c): well-rounded quartz and dolostone pebbles (2–3 cm), locally well-rounded dolostone cobbles (∅ up to 14 cm); *Acervulina*-corallinacean macroids (∅ 4–7 cm, c), laminar rhodoliths (∅ < 10 cm, c) | Bivalves: pectinids debris (<5 cm, r), ostreid fragments (r), steinkerns (1–2 cm, c); echinoids: *Echinolampas barchinensis* (r); foraminifer: *Amphistegina* (r); biserial textulariids (r), miliolids (r), globigerinids (s); bryozoans: celleporiforms (r) |

**Table 1** continued

| Section | Bed | Thickness | Lithology | Fossil content |
|---|---|---|---|---|
| | C2 | 2.4 m | Grey-brown corallinacean rudstone to floatstone with packstone matrix dominated by debris (∅ 0.5–2 mm) of thin encrusting corallinaceans (c) and fruticose growth forms (r) | Bivalves: *Pholadomya alpina* (c), *Periglypta miocaenica* (c), ostreid debris; branched and celleporiform bryozoans (0.5–1.5 cm, c); corals: delicate (ca. 3 mm) branched corals (probably *Stylocora*, r); foraminifers: *Amphistegina* (m), *Planostegina* (r), biserial textulariids (c) |
| | C3 | 1.2 m | Poorly sorted marly corallinacean rudstones to floatstones with packstone matrix dominated by debris (∅ 1–2 mm) of fruticose (c) growth forms containing *Acervulina* (r); at the top clay horizon (5-mm thickness) | Bryozoans: branched (∅ 1–2 mm, m), celleporiform (1–2 mm, m); bivalves: *Modiolus* (c), cardiids (c), pycnodont oysters (r), *Aequipecten malvinae* (c); foraminifers: *Amphistegina* (r), *Planostegina* (r), biserial textulariids (c), *Triloculina* (r), globigerinids (r) |
| | C4 | 2.1 m | Densely packed corallinacean rudstones, floatstones and packstones dominated by debris (∅ 1–3 mm) of fruticose growth forms | Bivalves: *Panopea menardi* (c), *Gigantopecten nodosiformis* (c), *Aequipecten malvinae* (c); *Hyotissa hyotis* (c), debris of pycnodont oysters (c); echinoid remains (c); *Thalassinoides* (∅ 1–2 cm, c); foraminifers: *Amphistegina* (m), textulariids (c), miliolids (r) |
| | C5 | 2.4 m | Porous corallinacean rudstone to floatstone with packstone matrix dominated by debris (∅ 2–4 mm) of fruticose (c) and thin encrusting (r) growth forms; *Acervulina* (r) | Bivalves: pycnodont oysters (c), *Aequipecten malvinae* (c), *Gigantopecten nodosiformis* (s); branched and celleporiform bryozoans (c); cirriped: *Pyrgoma multicostatum* (Seguenza, 1873; s); foraminifers: *Amphistegina* (c), *Sphaerogypsina* (r), biserial textulariids (c); *Thalassinoides* (∅ 1–2 cm, m) |
| | C6 | 1.2 m | Massive, densely packed corallinacean rudstone with packstone matrix dominated by debris (∅ 3–10 mm) of fruticose (c) and encrusting (r) growth forms and *Acervulina* (r); nodular rhodoliths (∅ 3 cm, s) | Corals: delicate branched (probably *Stylocora*, c); foraminifers: biserial textulariids (c), miliolids (r), *Amphistegina* (r) |
| | C7 | 3.1 m | Poorly sorted corallinacean rudstone with packstone matrix dominated by debris (∅ 2–8 mm) of fruticose and thin encrusting growth forms containing nodular rhodoliths (∅ 3–10 cm, c); *Acervulina* (r) | Bivalve: *Gigantopecten nodosiformis* (c); celleporiform bryozoans (c); echinoid debris (c); foraminifers: *Amphistegina* (r), *Triloculina* (r) |
| | C8 | 6.5 m | Massive corallinacean rudstone with packstone matrix dominated by debris (∅ 3–5 mm) of fruticose (c) and encrusting (c) growth forms; *Acervulina* (c) | Corals: *Porites* (c), delicate branched (probably *Stylocora*, c); gastropod and bivalve debris (<1 mm, c), steinkerns (<5 mm, c), *Cardium* (c); foraminifers: *Amphistegina* (c), textulariids (r), miliolids (r) |
| II | B1 | 0.3 m | Non-cemented, well-rounded but poorly sorted gravel consisting of granite-, quartz- and dolostone-pebbles (∅ 1–7 cm) and quartz-fine-sand | – |
| | B2 | 5 cm | Laminated mud- to wackestone | Bryozoans and corallinacean debris (c); *Amphistegina* (r) |
| | B3 | 1.5 m | Corallinacean rudstones to floatstones with mud- to wackestone matrix dominated by debris (∅ 0.5–1.5 cm) of laminated corallinaceans and rare well-rounded quartz and dolostone pebbles (∅ 2–3 cm); *Acervulina*-corallinacean macroids (∅ 4–7 cm); laminar rhodoliths (∅ 4–7 cm) | Branched bryozoans (r); foraminifers: *Amphistegina* (r), biserial textulariids (r), miliolids (r), globigerinids (s) |

**Table 1** continued

| Section | Bed | Thickness | Lithology | Fossil content |
|---|---|---|---|---|
| II | E0 | 0.4 m | Non-cemented, well-rounded but poorly sorted gravel consisting of granite-, quartz- and dolostone-pebbles (∅ 1–7 cm) and quartz-fine-sand | – |
| | E1 | 0.2 m | Calcareous middle- to fine-grained quartz-sandstone | – |
| | E2 | 0.4 m | Yellowish mudstone to wackestone with packstone areas dominated by corallinacean debris (<1 mm diameter) grading into a calcareous quartz-fine-sandstone; *Avervulina* (r) | Bivalves: shell fragments (<500 µm, c); bryozoans: celleporiform (r), branched (r); echinoid debris (r); foraminifer: *Amphistegina* (r) |
| | E3 | 0.1 m | Calcareous fine-grained quartz-sandstone and local clusters of quartz pebbles | – |
| | E4 | 1.2 m | Corallinacean rudstones to floatstones dominated by debris (∅ 2–4 mm) of laminated corallinaceans; *Acervulina*-corallinacean macroids (∅ 2–3 cm, c) | Bivalves: ostreid fragments, steinkerns (2–3 cm); echinoids debris (r); foraminifers: *Amphistegina* (r), biserial textularids (r), miliolids (r), globigerinids (s); bryozoans: branched (r) |

*s* Single, *r* rare, *c* common, *m* mass occurrence

In situ shells of *Pinna tetragona* are distributed throughout the bed but form a distinct horizon with densely spaced specimens (Fig. 8h) in the upper part of the bed where *Thalassinoides* burrows are also common. *Gigantopecten nodosiformis*, *Aequipecten malvinae* (du Bois de Montpereux, 1831), *Ctena decussata* and *Codakia* are typical bivalves. The bed is terminated by a thin silt-layer (bed 7a). A well-cemented corallinacean limestone (bed 8) follows, similar to bed 7, containing *Pinna tetragona* fragments. The bed is again terminated by a thin silty clay bed (8a). The following bed (bed 9; Fig. 4c), which is again terminated by a thin silty clay (bed 9a), is characterized by in situ *Pinna tetragona*, especially at the base. *Thalassinoides* burrows and cardiids are very common; disarticulated shells of *Gigantopecten nodosiformis* are found in the entire bed. There is a change to a massive limestone (Fig. 4c), which contains abundant *Periglypta miocaenica*, especially in the basal part along with *Glycymeris deshayesi*, while *Pinna tetragona* occurs only at the base. A fining-upward trend is documented by the development of fine-grained limestones at the top. Ca. 100 m to the N, the bed becomes more porous. It is followed by two beds (11 and 12) that are characterized by poorly cemented corallinacean limestones with common shells of *Gigantopecten nodosiformis* (e.g., at the base of bed 11, commonly affected by sponge borings) and *Glycymeris deshayesi*. *Pinna tetragona* rarely occurs in situ (bed 12). Bed 11 can be clearly discriminated from bed 12 by its soft chalky appearance. Bed 12 is overlain by a corallinacean limestone (bed 13), characterized by numerous *Amphistegina* in the lower part, which are disappearing abruptly after ca. 7 m. Bryozoans and serpulids (horizon of ca. 25 cm) are common 6 m above the base. The amount of *Amphistegina* increases toward the top. The same bed pinches out to ca. 500 m to the ENE directly onlapping onto the dolostone. It is represented by two horizons consisting of corallinacean limestones characterized by mass occurrences of *Amphistegina*. Section I is terminated by a massive corallinacean limestone, similar to bed 1 in its faunal content.

## Section II

The base of section II (Figs. 3, 4d) is made up of a dark-grey massive dolostone, which crops out only in the northern part of the Mannersdorf quarry area with a total height of ca. 30 m in unconformable contact to overlying beds. With a gap of ca. 2 m above the dolostone, section II starts with a white silt layer (bed 1) followed by a succession of three monomictic dolostone breccia beds, onlapping on the dolostone. The lowest breccia (bed 2) consists of subangular components up to 20 cm, while the components of the middle layer (bed 3) are smaller (5–7 cm) and the bed shows a fining-upward trend with

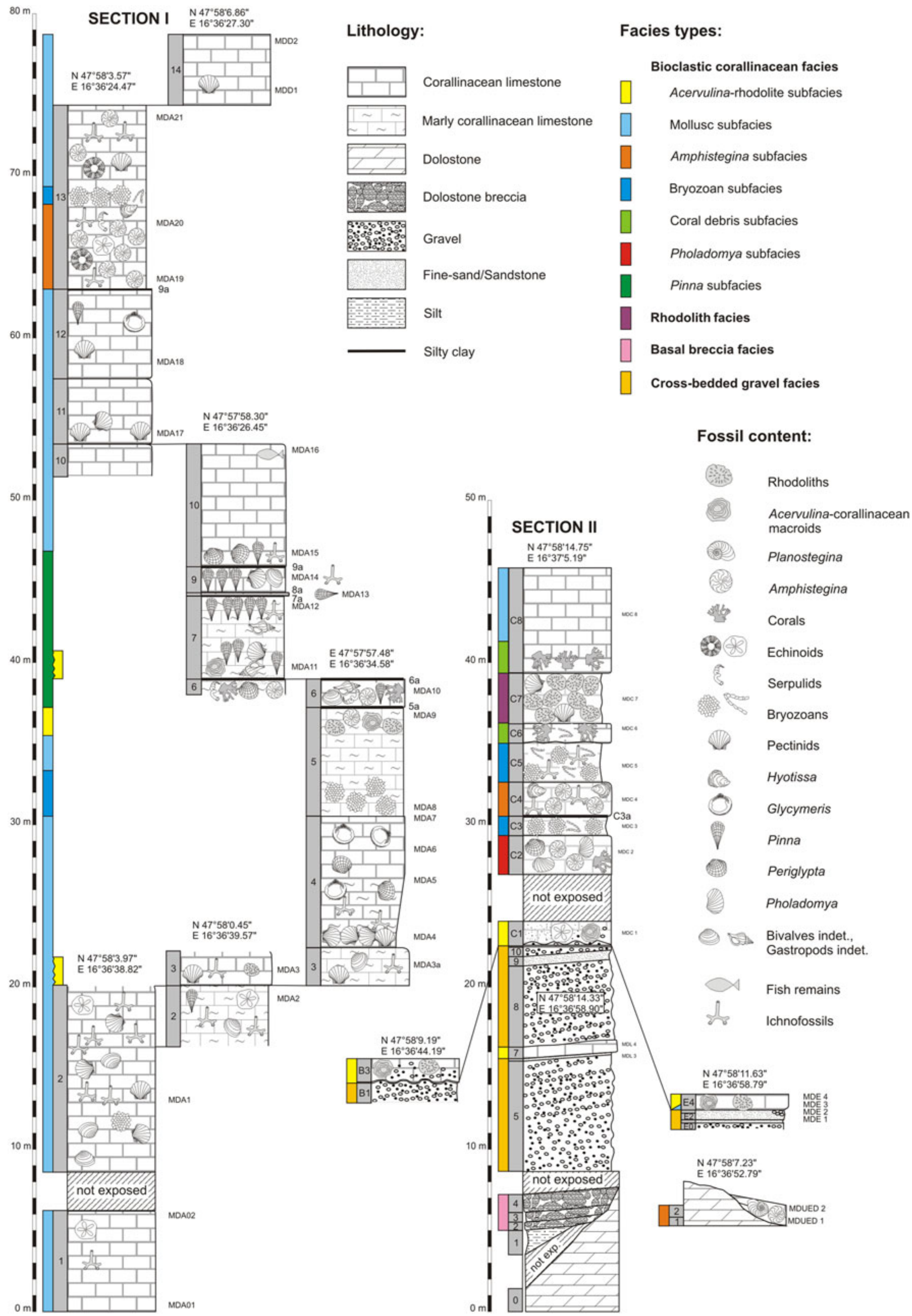


**Fig. 3** Lithologic columns of sections I and II including sample numbers and GPS coordinates. *Colors* represent facies types

increasing amounts of silty sand in the topmost 5–8 cm. The uppermost breccia layer (bed 4), displays a fining-upward trend as well, ranging from components of 3–5 cm in diameter in the basal 30 cm to components of 1–2 cm in size in the upper part. The components at the base are better rounded than those of the lower and middle breccia bed and show bioerosion of *Entobia*. The transition from the onlapping breccias to the gravels (bed 5) is covered by soil. About 15 m of [non-cemented] gravel (Fig. 4d) is exposed, which develop foresets in the upper part of bed 5 with a dip of ca. 20° to the NW. The gravel is well rounded but poorly sorted with alternating coarse and fine layers. It is terminated by a ca. 20-cm-thick iron-crust containing well-rounded quartz pebbles. The crust is overlain by 10–15 cm of calcareous quartz-fine-sandstone (bed 6). Above follows a marly corallinacean limestone (bed 7) dominated by fragments of corallinaceans with laminar growth forms. Well-rounded quartz pebbles are common in the lower part and above there is about 7 m of gravels (bed 8) that show clear foresets in the lower part. Sand content increases continuously to the top reaching up to 50%; sorting of the gravel also increases. Ca. 5 m above the corallinacean limestone bed, a fine-sand layer (bed 9) is developed. Also some local fine-sand lenses with 0.1–0.5 m length and 1–2 cm thickness are dispersed within the gravel, e.g., directly below the corallinacean limestone (bed C1), which terminates the gravel. Ca. 400 m further SW, the gravels crop out (B1), directly followed by corallinacean limestones containing dolostone cobbles with dimensions of up to 14 cm. The boundary between gravel (Fig. 5b) and limestones is mostly an unconformity (also cropping out ca. 400 m in the SW) but conformable contacts are also present (e.g., ca. 160 m in the S and ca. 260 m in the SW). It shows a dome-shaped topography (cupolas) with diameters of ca. 30 cm. Mudstone and partly wackestone horizons with variable thickness (1–15 cm) are locally developed between the corallinacean limestones and the gravel. Internally, the wackestones are laminated containing bryozoan and corallinacean debris and scattered *Amphistegina*. A differently developed boundary can be found ca. 150 m in the SSW where the gravel (bed E0) is followed by a calcareous middle- to fine-grained sandstone (bed E1), yellowish mudstones to wackestones with packstone areas covered by calcareous fine-sandstone E2, calcareous fine-grained sandstones (bed E3) with clusters of quartz pebbles and corallinacean limestones (bed E4). The first limestone bed above the gravel (C1, B3, and E4, see Fig. 3) consists of corallinacean limestones with common encrusting corallinaceans. Well-rounded scattered quartz and dolostone pebbles, some cm in diameter, can also be detected, especially in the lower part of the bed. Close to the dolostone (ca. 90 m to the SW), well-rounded dolostone cobbles (up to 14 cm diameter) with sponge borings occur. In B3, the corallinaceans occasionally bind quartz grains. *Acervulina*-corallinacean macroids are common as well as laminar rhodoliths of the same size. The contact of bed C1 to bed C2 is not exposed. The outcropping bed consists of a corallinacean limestone. Steinkerns (10–15 cm) of *Pholadomya alpina* (Matheron, 1842) and *Periglypta miocaenica* are very common, along with shell debris of ostreids. In southern direction, debris of delicate (ca. 3 mm) branched corals (probably *Stylocora*) occurs. Branched and celleporiform bryozoans commonly occur, occasionally encrusted by corallinaceans forming thick-branched rhodoliths. The mass occurrence of *Amphistegina* and the prominence of thin encrusting corallinaceans in layer C2 distinguishes it very clearly from the following bed. Bed C3 (Fig. 5a), which is characterized by a high marly content, locally shows mass occurrences of branched and celleporiform bryozoans. Up-section, the bed becomes more porous and grades into a clay layer (ca. 5 mm in thickness). *Modiolus*, cardiids, pycnodont oysters, and *Aequipecten malvinae* are typical bivalves. In contrast, the following bed (C4; Fig. 5a) shows mass occurrences of *Amphistegina* and *Panopea menardi* (Deshayes, 1828) which can be found in life position at the base. Fragments of bivalves are common; at the top, well-preserved shells of *Hyotissa hyotis* (Linnaeus, 1758) occur. Up-section a highly bioturbated and poorly sorted corallinacean limestone follows (bed C5; Fig. 5a), which is nearly identical to bed C3. The contact to bed C6 is unconformable (Fig. 5a). Bed C6 (Fig. 5a) is a massive, densely packed, prominently exposed corallinacean limestone containing debris of delicate (ca. 3 mm) branched corals. It is overlain by a poorly cemented corallinacean limestone (C7; Fig. 5a) that contains many nodular rhodoliths (∅ 3–10 cm), which are densely packed or occasionally float in a matrix of corallinacean debris. Celleporiform bryozoans are commonly encrusted by corallinaceans or *Acervulina*. The top of the section (C8; Fig. 5a) is formed by a massive corallinacean limestone that contains common thin-branched (ca. 1 cm) *Porites* and debris of delicate branched (ca. 3 mm) corals

**Fig. 4** Phototransects with bed numbers documenting facies zonations (highlighted in *colors*) and fossils (legends follow Fig. 3). Section I is represented by (**a–c**), section II by (**d**) and Fig. 5a–c. Positions of phototransects are marked in Fig. 2. **a** Phototransect I—Part 1, NNE–SSW oriented. A fault plane is illustrated by the *shaded field*. The hanging wall at the right is represented by bed 2. **b** Phototransect I—Part 2, NNE–SSW oriented. Bed 3 (*yellow*) onlaps on bed 2, which shows a flexure with a height of ca. 5 m. **c** Phototransect II, ESE–WNW oriented. Horizontal bedding with a lateral facies change from the *Pinna* subfacies to the mollusc subfacies. **d** Phototransect III, N–S oriented. The basement (dolostone) is overlain by a breccia (1–4). It is followed by cross-bedded gravels (5, 8–10) with a corallinacean limestone intercalation (6–7). At the top corallinacean limestones (C1) are developed ▶

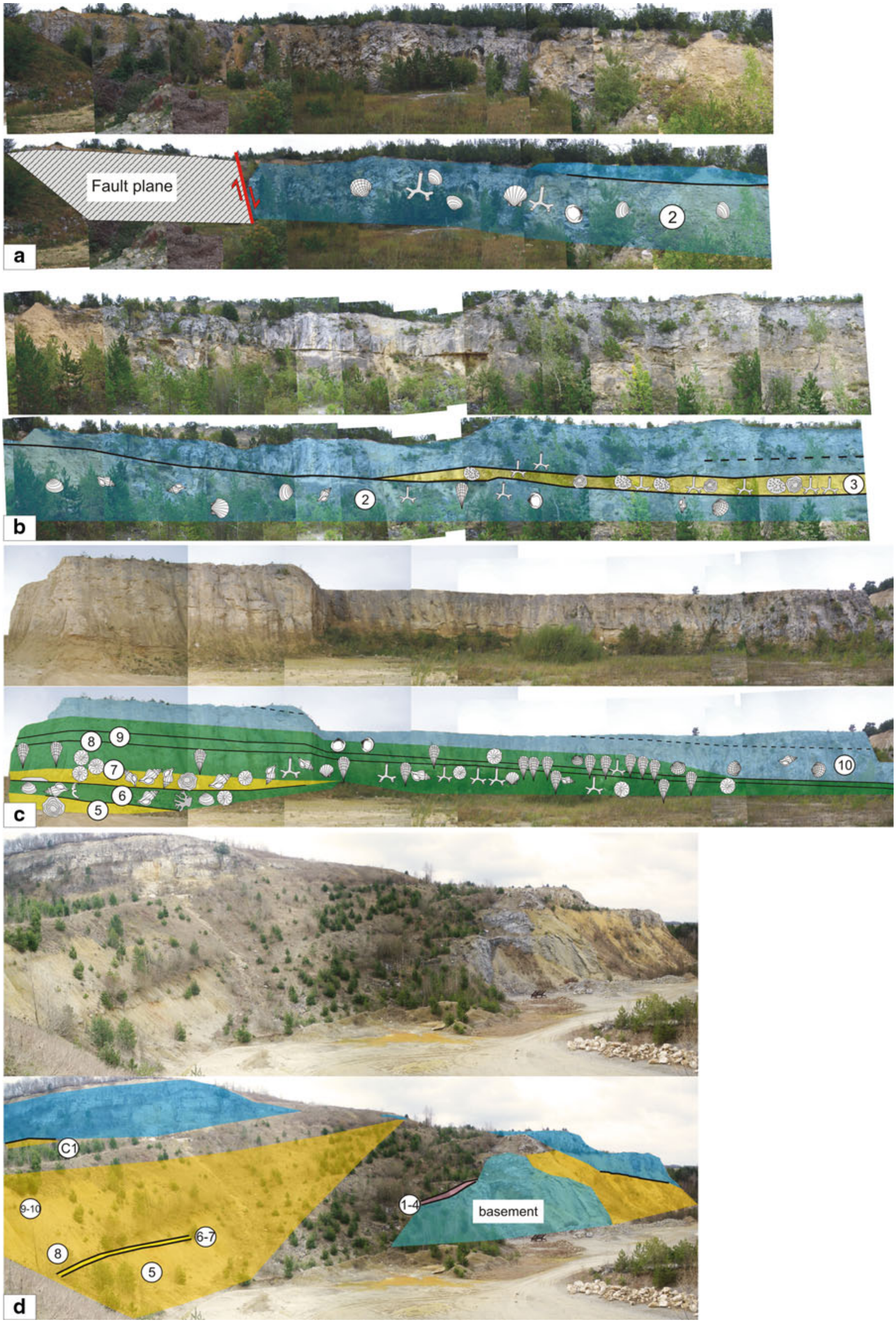
Fault plane
2
a
2
3
b
8
9
7
6
5
10
c
C1
9-10
8
6-7
5
1-4
basement
d

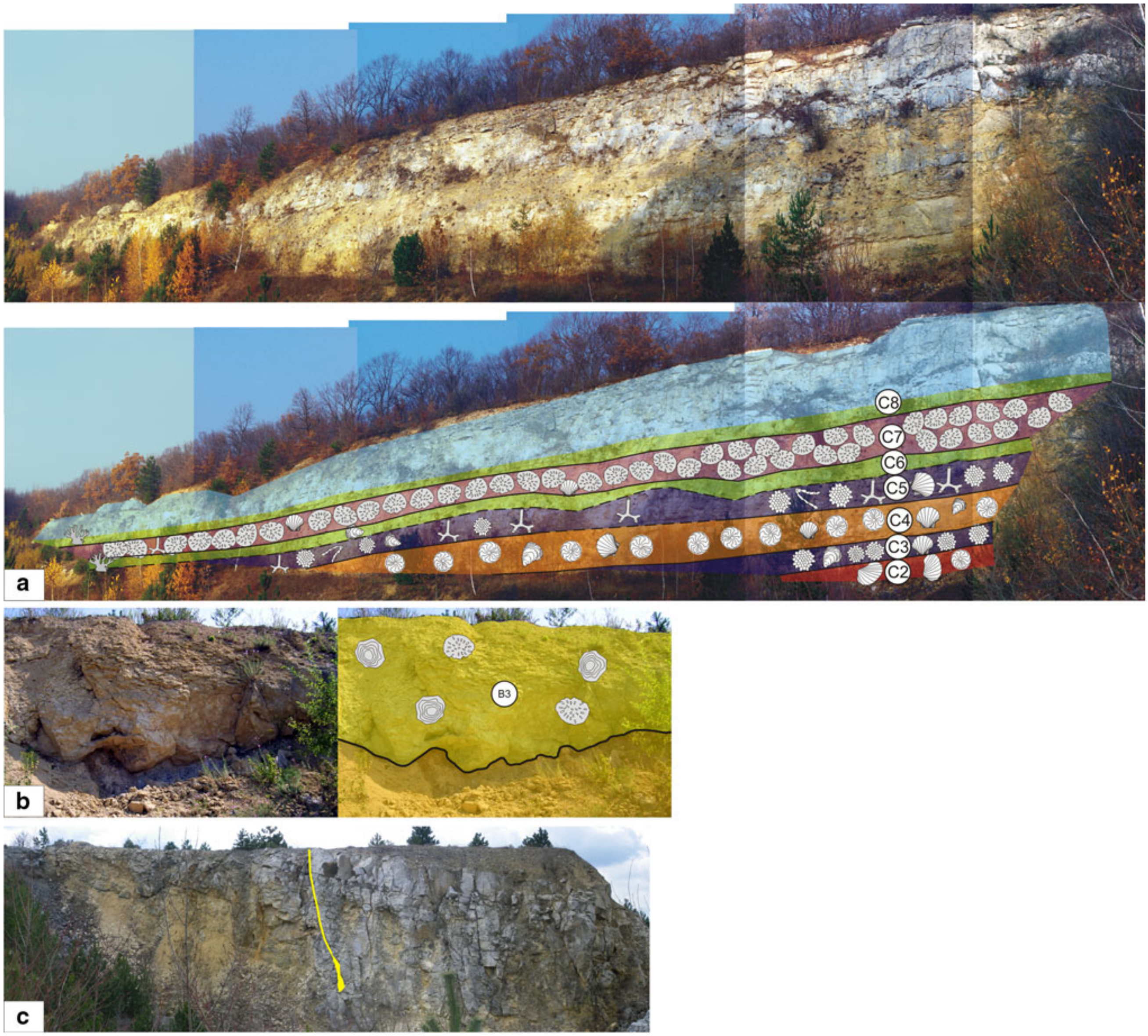


**Fig. 5** Phototransects with bed numbers documenting facies zonations (highlighted in *colors*) and fossils (legends follow Fig. 3). Section I is represented by Fig. 4a–c, section II by Fig. 4d and (**a–c**). Positions of phototransects are marked in Fig. 2. **a** Phototransect IV, NNW–SSE oriented. Corallinacean limestones show horizontal bedding. Between bed C5 and C6 an unconformity is present. **b** Phototransect V, NNW–SSE oriented. Unconformity between gravel (base) and corallinacean limestone (*top*). **c** Phototransect VI, NW–SE oriented. Jointset fillings are highlighted in *yellow*

at the base. Bivalves and gastropods are common in this bed, as are *Amphistegina* and *Acervulina*.

## Tectonics

A fault (indicated in Figs. 2, 4a) divides the quarry area into two blocks; the southwestern block acts as a hanging wall. A vertical displacement of the blocks of at least 20 m can be estimated. The fault plane has a mean dip angle of 56° with a mean dip direction of 251°. The surface is smoothly polished; locally the footwall is covered by a few-cm-thick flowstone. Two types of slickensides are present, the first slip-line gives a mean value of 53°/258° (plunge/azimuth); the second a mean value of 25°/333°. Close to the fault plane, bed 2 shows a slight flexure with a height of ca. 5 m at the deepest point (Fig. 4b). The first slip-line indicates ENE–WSW extension, the second, younger lineation documents a reactivation as a dextral strike-slip fault (Fig. 6a–b). Orientations of the principal stress axes (dip angle/dip direction) are given by $\sigma 1$ (79/042, 90/000), $\sigma 2$ (05/160, 00/090) and $\sigma 3$ (10/251, 00/000). Within section II, close to the fault (N 47°58′10.07″, E 16°36′52.48″),

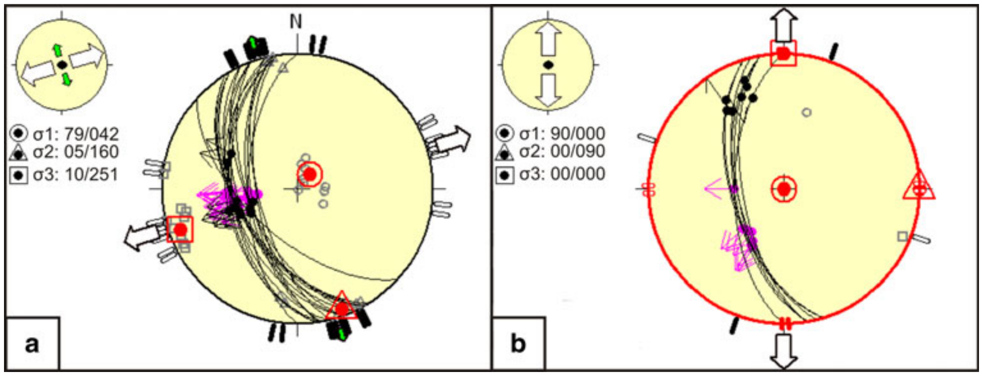


**Fig. 6** Stereographic representation of the fault and its paleostress orientations. The fault plane is shown as cyclographic trace with associated slip lines; normal fault is given by a *dot with outward arrow* for normal faulting. Stress inversion results are represented by $\sigma1$ (*dot surrounded by circle*), $\sigma2$ (*triangle*) and $\sigma3$ (*square*). The *small circle* on the *upper left corner* of the figures symbolizes the vertical stress ($\sigma$v), in this case representing extensional regimes ($\sigma1 \approx \sigma$v). *Green arrow*: $\sigma2$ is subhorizontal; *white arrow*: $\sigma3$ is subhorizontal; *outward arrow*: extensional deviatoric stress. The fault represents two differently oriented extensions. **a** ENE–WSW-trending extension (slip-line 1). **b** N–S-trending extension (slip-line 2)

the limestone beds C2-C4 are pervaded by a closely spaced vertical jointset with 10 to 100-cm-wide open fractures (Figs. 5c, 9c). The joints are filled with well-cemented thin-layered (mm thick) marly packstones to wacke- and mudstones. The layers show repeated fining-upward sequences (ca. 1–2 cm). Corallinacean debris is common; *Amphistegina*, echinoid spines and *Planostegina* are rare. Also reworked limestone clasts (ca. 2 mm), consisting of grainstones with mollusc and corallinacean fragments, commonly occur (Fig. 9d).

## Facies analysis and interpretation

Ten facies types, including subfacies types, have been distinguished based on lithological and paleontological characters. The spatial relationship between the facies is indicated in Fig. 10.

### Basal breccia facies

The basal breccia facies (Fig. 7a, b) consists of a monomictic dolostone breccia. Components are subangular and between 1 and 20 cm. Fining-upward sequences are developed in this facies, which is seen in beds 2–4 of section II. The matrix is a silty fine-sand. Towards the top of the fining-upward sequence, the amount of matrix increases. *Gastrochaenolites* (clavate borings) and *Entobia* (chambers with small channels) within the dolostone clasts are common. The facies directly follows above the dolostone and is overlain by the cross-bedded gravel facies.

Interpretation: The subangular components indicate very short transport within a turbulent water body. A marine environment is evident due to the occurrence of borings, which are referred to the bivalve *Lithophaga* and to clionid sponges. The facies is interpreted as coastal slope scree with breccias in a few meters water depth originating from the rocky shore formed by a dolostone cliff.

### Cross-bedded gravel facies

The cross-bedded gravel facies (Fig. 7c, d) is exposed in section II and consists of well-rounded but poorly sorted polymict gravel (1–7 cm) composed of metamorphic and pegmatitic rocks (Fencl 2005). They are supported by fine-grained quartz-sand reaching 50–70% and occasionally clay up to 25%. Quartz fine-sand layers or dispersed fine-sand lenses of variable thickness (cm to dm) are intercalated within the gravels. The whole succession shows cross-bedding with a dip of ca. 20° to the NW. Within this facies, a limestone bed of the *Acervulina*-rhodolith facies is intercalated, the latter also terminates the cross-bedded gravel facies.

Interpretation: The gravels, which derive from Lower Austroalpine tectonic units (Fencl 2005), are poorly sorted but well rounded with a high fine-sand content. The high degree of roundness indicates a long transport and/or subsequent coastal reworking. The exact provenience of the gravels is still unclear; the source area may be the basement of the Leitha Mountains itself, as part of the Semmering Quartzite (Tollmann 1976). River transport but also marine reworking by coastal breakers in a deltaic system has been discussed by Sohs (1963) and Fencl (2005) and the cross-beddings have been interpreted as foresets (Fencl 2005) originating from a prograding river delta. Marine reworking may be indicated in the uppermost part of the gravel successions, where clear foresets are missing. The dip of the foresets (ca. 20°) indicates a steep alluvial cone of relatively small radius; such characteristics point to a fan delta (cf. McPherson et al. 1987) most likely of Gilbert-type (Postma 1990). The limestone bed within the gravels reports an interruption of river progradation and a slight deepening, maybe during a marine transgression or temporal change in river discharge. In a similar depositional setting, corallinacean limestones formed above a drowned Gilbert-type delta in a water depth of 10–20 m (García-García et al. 2006).

*Bioclastic corallinacean facies*

In this study, the bioclastic corallinacean facies is a unit subsuming sediments predominantly composed of unattached coralline algal branches, rhodoliths, and their detritus and is therefore very similar to maërl described from many modern environments (e.g., Cabioch 1968; Keegan 1974; Adey 1986; Steneck 1986; Freiwald et al. 1991; Freiwald 1994). It is neutral in terms of represented coralline algal species, however, it is similar to the *Lithothamnium* facies of Bosence (1976) although *Lithothamnion* is not dominating, and is not defined by certain grain sizes, as for example the algal gravel facies (Schlanger and Johnson 1969). The facies comprises packstones, rudstones, and floatstones consisting of angular and sub-rounded corallinacean clasts of fruticose or encrusting growth forms. The corallinaceans are represented by *Lithothamnion*, *Spongites*, *Mesophyllum*, *Lithophyllum*, and *Sporolithon*. Occasionally, rhodoliths or *Acervulina*-corallinacean macroids occur. Bivalves and gastropods occur in variable amounts, as well as regular and irregular echinoids and bryozoans, which are represented by celleporiform, branching, or crustose growth forms. Foraminifers are represented by rotaliids, such as *Amphistegina*, *Planostegina*, *Asterigerina*, and common cibicidoids, biserial textulariids, miliolids (e.g., *Triloculina*), and rarely globigerinids. The heterogeneity of this facies allows the definition of subfacies types that can be discriminated by the abundance of certain biogenic components and textural differences. Similar Recent sediments occur e.g., in rather low-energy and clear waters of the Mediterranean Sea down to 40 m (Rasser 2000 and further references therein), and in very shallow (<10 m) environments, e.g., the Gulf of California (Schlanger and Johnson 1969; Halfar et al. 2004).

*Acervulina-rhodolith subfacies*

The *Acervulina*-rhodolith subfacies (Fig. 7e, f) is represented by rudstones and floatstones with a packstone matrix and exhibits sub-rounded corallinacean debris (2–5 mm), *Acervulina*-corallinacean macroids (3–5 cm), and laminar spheroidal to ellipsoidal rhodoliths (5–7 cm) with warty surface. The bioclasts of the packstone matrix are poorly sorted consisting of fine-grained debris of corallinaceans, molluscs, and foraminifers. Corallinaceans are dominated by fruticose and encrusting growth forms; thin encrusting growth forms are common. Foraminifers are represented by rotaliids (e.g., *Amphistegina*), biserial textulariids, miliolids, and rare globigerinids. Rare celleporiform bryozoans are commonly encrusted by corallinaceans. Fragments of echinoids rarely occur. The *Acervulina*-rhodolith subfacies is developed in section I (beds 3, 5, 7) and section II (beds C1, B3 and E4). The facies is also intercalated within the cross-bedded gravel facies and associated with the mollusc subfacies and the *Pinna* subfacies.

Interpretation: The *Avervulina*-rhodolith subfacies shows similarities with the mollusc subfacies but exhibits a high amount of *Acervulina*-corallinacean macroids. It is similar to the bioclastic rhodolith debris facies of Dullo (1983). Also, corallinacean rudstones and rhodolith floatstones from the Burdigalian of the Latium-Abruzzi Platform (Brandano and Piller 2010) or Eocene limestones of the Maritime Alps, where *Acervulina*-corallinacean macroids and rhodoliths occur together (Varrone and D'Atri 2007), are similar to this facies.

Pebble- to cobble-sized macroids of *Acervulina inhaerens* (Schultze, 1854), together with corallinaceans are reported from Pacific fore-reef to island shelf areas from approximately 50–150 m depth (Iryu et al. 1995) and also from 60 to 100 m depth (Bassi and Humblet 2011). In the northern Red Sea, *Acervulina inhaerens* occurs from 5 to 50 m, but is dominant below 40 m (Rasser and Piller 1997). Fossil acervulinid macroids are also indicative of environments around 40–50 m (cf. Hottinger 1983; Reid and Macintyre 1988; Prager and Ginsburg 1989; Varrone and D'Atri 2007). Settings with higher water energy for formation of acervulinid macroids are discussed in Perrin (1994) and Varrone and D'Atri (2007).

Although common occurrences of *Acervulina* often indicate deeper water, their dependence on symbionts restricts them to clear water conditions (Hottinger 1983). The occurrence of *Acervulina* in section II (always directly above the gravels) may be caused by turbid water conditions, in which they outcompete corallinaceans (Bosellini

**Fig. 7** Basal breccia facies. **a** Onlap of Badenian dolostone breccias onto Triassic dolostone. **b** Monomictic dolostone breccia with subangular components (1–20 cm) with internal fining-upward trend. **c–d** Cross-bedded gravel facies. **c** Well-rounded poorly sorted fine-sand-supported gravel (ca. 5–7 cm) overlain by corallinacean limestone with dome-shaped topography (cupola) in between. **d** Cross-bedded gravel of bed 5 with high amounts of quartz (Q) and paragneiss (P). **e–f** *Acervulina*-rhodolith subfacies. **e** *Acervulina*-corallinacean macroid of section II (bed B3). **f** Corallinacean rudstone (same bed as **e**) containing ellipsoidal rhodoliths (ca. 7-cm length) and quartz grains (Q). **g–h** Mollusc subfacies. **g** Encrusting red algae developed around a calcitic bivalve shell (M), which was bored and filled with peloids (P) after encrustation, showing geopetal fabrics (G). **h** Corallinacean packstone containing gastropods (G) and textulariids (T) ▶

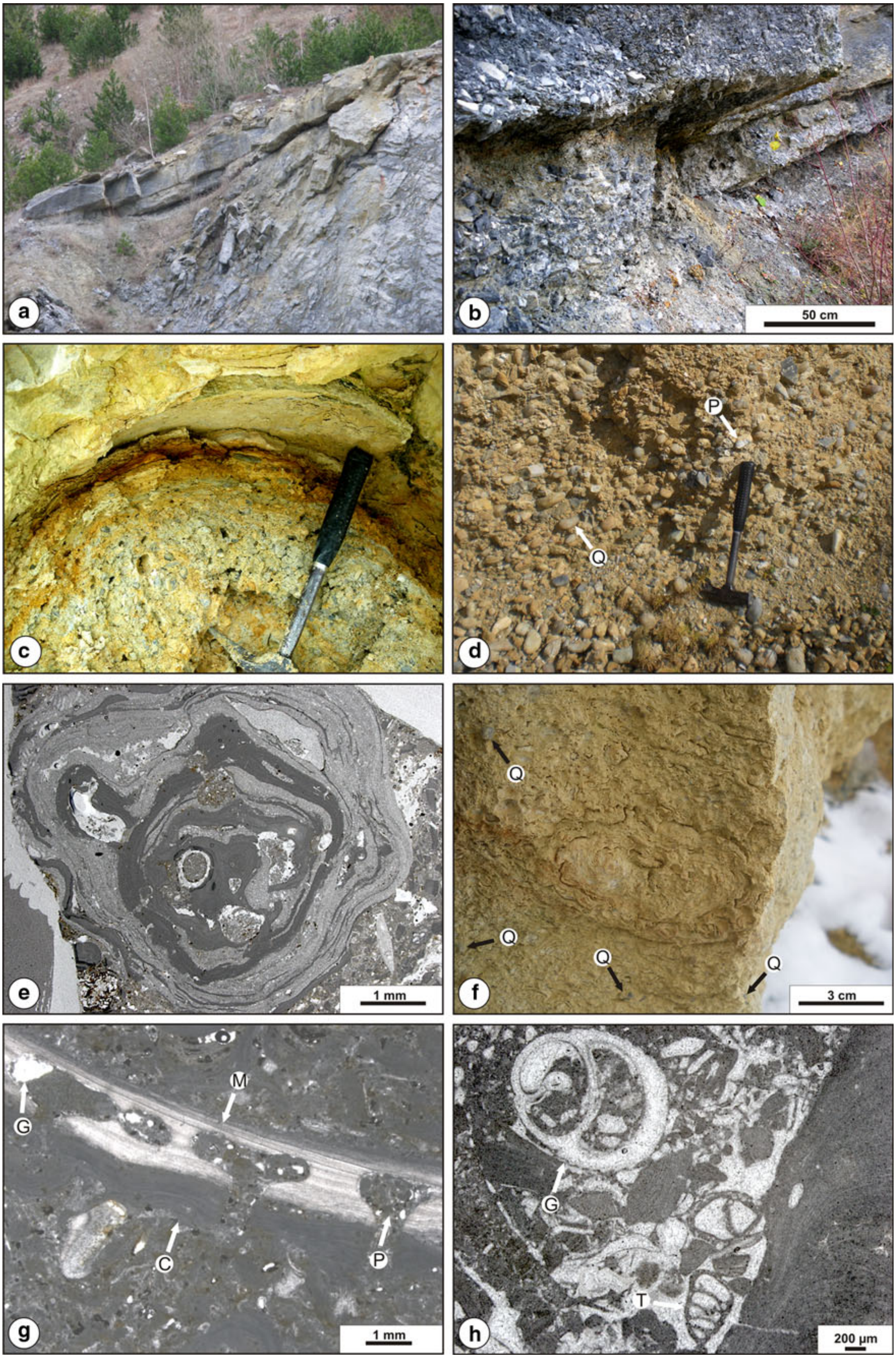
a
b
50 cm
c
P
Q
d
Q
e
1 mm
Q
Q
Q
f
3 cm
G
M
C
P
g
1 mm
G
T
h
200 µm

and Papazzoni 2003) and make a considerably shallower water depth very likely. The intercalation of this facies within the cross-bedded gravel facies suggests a water depth of 10–20 m (see above).

Corallinacean limestones characterized by this facies locally show unconformities at the contact to the cross-bedded gravels (Fig. 5b). The limestones show influence of freshwater diagenesis, which is indicated by completely dissolved and newly formed crystals that build a mosaic destroying former structures. Such phenomena are influenced by the freshwater phreatic zone (e.g., Dullo 1983). The limestones show dome-shaped topographies (cupolas) at the bottom side of the bed. These structures, in combination with freshwater diagenesis of the limestone bed, indicate groundwater influence and very likely a hypogenic speleogenesis with hydrothermal influence (Klimcouk 2007). Hydrothermal influence in interaction with hypogenic speleogenesis has already been documented for a cave south of the Baxa Quarry (Plan et al. 2006). The gravels of the Mannersdorf quarry area in that way acted as an aquifer. Interspace between gravels and limestones probably vanished due to compaction load. Iron-crusts, which occur in section II, are occasionally of synsedimentary or postsedimentary origin formed along fluid diffusion passages associated with microbial processes (Baskar et al. 2008), occasionally under hydrothermal influence (Konhauser and Ferris 1996).

*Mollusc subfacies*

The mollusc subfacies (Fig. 7g, h) comprises rudstones and floatstones that are characterized by high amounts of various molluscs. The corallinaceans are dominated by corallinacean debris with fruticose growth forms (2–5 mm). Occasionally, fragments (200–400 µm) of thin encrusting growth forms are abundant. Mollusc shells are commonly encrusted and often strongly bioeroded before or after encrustation (Fig. 7g). The borings are frequently filled with peloids (Fig. 7g). Aragonitic shells are often dissolved and replaced by sparite. Small thin-shelled bivalves are common in this facies. Foraminifers are represented by rotaliids (*Amphistegina*, *Planostegina*), biserial textulariids, miliolids (e.g., *Triloculina*), and rare globigerinids. Bryozoans (100–200 µm) are rare. The facies is characterized by strong bioturbation; occasionally *Thalassinoides* burrows are preserved. Bivalves are represented by ostreids (e.g., *Hyotissa hyotis* and *Ostrea*), pectinids (*Gigantopecten nodosiformis*), cardiids (*Cardium*), venerids (*Periglypta miocaenica*), glycymeridids (*Glycymeris deshayesi*) and lucinids (*Codakia*). Pectinids are usually disarticulated and randomly distributed. Locally, they form distinct coquinas. In most cases, they are highly bioeroded by sponges and bivalves. Bivalves are commonly articulated and preserved in situ. Gastropods are mainly represented by steinkerns of *Conus*, *Trochus*, *Cerithium*, *Xenophora*, and *Turritella*. Cidarids are usually fragmented, while irregular echinoids are well preserved. Cirripedians, polychaetes, and fish teeth occur in negligible amounts. The mollusc subfacies characterizes beds 1–5 and 10–14 in section I and beds E4, and the upper part of C8 in section II. The facies is associated with the *Acervulina*-rhodolith subfacies and the bryozoan subfacies.

Interpretation: The facies is equivalent to the bioclastic algal mollusc facies of Dullo (1983) and to the branching algae facies of Studencki (1988, 1999) with its diversified molluscan assemblage. Also, the branch-dominated facies of Basso et al. (2008) is similar to this facies. The packstone areas have strong similarities to the bioclastic algal debris facies of Dullo (1983) and the algal branch packstone facies and algal debris wackestone facies of Bosence and Pedley (1979). The packstone areas, consisting of fine-grained bioclastic algal debris, indicate locally high bioturbation (Bosence and Pedley 1982).

Zuschin and Hohenegger (1998), Zuschin et al. (2009), and Jannsen et al. (2011) describe comparable mollusc assemblages from the modern Red Sea. There, turritellids are widely distributed on soft and hard substrates, muddy sediments, and on the reef slope down to 40 m; cerithiids show distinct habitat preferences and occur in water depths between 1 and 40 m with common occurrences between 5 and 30 m, while xenophorids are common in depths between 40 and 50 m (Jannsen et al. 2011). Trochids are abundant in samples from seagrass meadows, reef slopes, and sands between coral patches in depths around 5–20 m (Zuschin et al. 2009).

*Glycymeris* is documented from sands between coral patches in depth of ca. 10 m (Zuschin and Hohenegger 1998). Glycymerids and *Periglypta* are also reported from present-day sand bottoms at 10–30 m depth from the Florida Keys (Mikkelsen and Bieler 2008).

The mollusc subfacies is often associated with the *Acervulina*-rhodolith subfacies and the bryozoan subfacies in section I. A similar association has been described by Studencki (1999), who mentions a linkage to the relatively deeper algal-bryozoan facies. The mollusc subfacies very likely represents a shallow transition zone between shallower regimes (*Acervulina*-rhodolith subfacies, see above) and relatively deeper water leading to the bryozoan subfacies (see below). Aside from subtropic faunal elements, modern analogues are coralline algal deposits in the bays of Naples and Pozzuoli in the Mediterranean area (Toscano et al. 2006).

*Amphistegina subfacies*

The *Amphistegina* subfacies (Fig. 8a, b) comprises poorly sorted corallinacean rudstones and floatstones dominated by fragments of fruticose (1–3 mm) and thin encrusting growth forms. The interspace between mostly highly fragmented corallinaceans is filled with corallinacean pack- or wackestones. Mass occurrences of *Amphistegina* are name-giving for this facies. Occasionally, *Amphistegina* is associated with *Planostegina*. Biserial textulariids are common; miliolids are rare. Larger bivalves are represented by *Gigantopecten nodosiformis*, *Glycymeris deshayesi*, and *Panopea menardi*. Branched and celleporiform bryozoans occur in low amounts. Regular and irregular echinoids are rare. The facies is developed in the lower part of bed 13 of section I, in bed C4 of section II and in the beds, which onlap onto the dolostone. It is associated with the bryozoan subfacies.

Interpretation: The *Amphistegina* subfacies is similar to the *Pinna* subfacies and *Pholadomya* subfacies in its microfacies but is characterized by the very common occurrence of *Amphistegina*. Recent *Amphistegina* inhabits the tropical to subtropical belt in shallow waters down to 70–80 m (Larsen 1976) where it is primarily attached to macrophytes with high densities (Fujita et al. 2009). Its presence implies a minimum water temperature of 17°C (Adams et al. 1990; Betzler et al. 1995). Some living *Planostegina* inhabit commonly water depths between 15 and 45 m, while others have highest abundances below this depth (cf. Hohenegger et al. 2000; Renema 2006 and further references therein). A typical bivalve of this facies is the deep-burrowing *Panopea menardi*, which occurs in life position (e.g., section II). Modern representatives of *Panopea* live in sandy and muddy substrates preferring shallow subtidal habitats down to 20 m, burrowing between 0.6 and 2 m depth into the sediment (Yonge 1971; Ludbrook and Gowlett-Holmes 1989). A similar facies is present in Badenian corallinacean limestones of Croatia (Basso et al. 2008).

In summary, the *Amphistegina* subfacies has been formed in a shallow, sublittoral environment with a depth range of ca. 20–30 m between the bryozoan subfacies and the mollusc subfacies (Fig. 4).

*Bryozoan subfacies*

The bryozoan subfacies (Fig. 8c, d) consists of poorly sorted, densely packed rudstones and floatstones. They are dominated by debris of fruticose and encrusting corallinaceans (ca. 3–5 mm). Branched or celleporiform bryozoan colonies (in general ca. 2 mm) are abundant. The bryozoans often form bryoliths of 30–50 mm in diameter, occasionally encrusted by *Acervulina*. Interspaces are filled with bioclastic pack- or wackestones. Rare echinoids are highly fragmented. *Thalassinoides* burrows are common. Foraminifers are represented by common biserial textulariids, miliolids (*Triloculina*), rotaliids (*Amphistegina*) and very rare globigerinids. Molluscs are represented by *Modiolus*, *Gigantopecten nodosiformis*, and ostreids. The facies is developed in section I (bed 5 and 13) and section II (bed C3 and C5). The facies is associated with the *Pholadomya* subfacies and the *Amphistegina* subfacies.

Interpretation: The bryozoan subfacies is similar to the algal-bryozoan facies of Studencki (1988, 1999) but Studencki's facies contain a rich bivalve and brachiopod assemblage. The formation of bryoliths is comparable to that of rhodoliths (James et al. 2006) and similar hydrodynamic conditions can be assumed. The sphericity in bryoliths is thought to be in part related to the turning frequency (Rider and Enrico 1979); Barbera et al. (1978) interpreted similar sediments as shallow deposits with sufficient water energy for rhodolith movement. A depth estimate of ca. 30 m is given by Studencki (1988). Modern analogues are found on the Apulian shelf along the shore in ca. 10–30 m water depth (Sarà 1969; Toscano and Sorgente 2002). The bryozoan subfacies is associated with the *Amphistegina* subfacies (section I, section II), the *Pholadomya* subfacies (section II), the mollusc subfacies (section I) and the coral debris subfacies (section II). A water depth deeper than that of the mollusc subfacies can be assumed.

*Coral debris subfacies*

The coral debris subfacies (Fig. 8e1–e2) comprises moderately sorted corallinacean-coral rudstones. The corallinaceans are dominated by debris (3–10 mm) of fruticose growth forms but thin encrusting corallinaceans or encrusting foraminifera (*Acervulina*) are also common. The corals are represented by *Porites* and delicate (ca. 3 mm in diameter) branched corals. The corals are usually fragmented; in situ colonies of *Porites* are less common. Corals are often encrusted by corallinaceans. Foraminifers occur in variable amounts, occasionally dominated by biserial textulariids and miliolids, occasionally by rotaliids (*Amphistegina*). The associated bivalve fauna is dominated by ostreids (mainly *Hyotissa hyotis* and *Ostrea*), pectinids, such as *Gigantopecten nodosiformis*, cardiids (*Cardium*), venerids (*Periglypta miocaenica*), glycymeridids (*Glycymeris deshayesi*) and lucinids (*Codakia*). Gastropods are represented by *Conus* and *Cerithium*. Associated with the corals is the cirriped *Pyrgoma multicostatum*. The facies occurs in section II (bed 2 as small patches, bed 6 and 8) and is associated with the rhodolith facies.

Interpretation: The coral debris subfacies is similar to the mollusc subfacies in its microfacies and is an equivalent of the modern bivalve/coral-communities of Riegl and Piller (2000) and the 'coral-red algal rudstone-floatstone' of

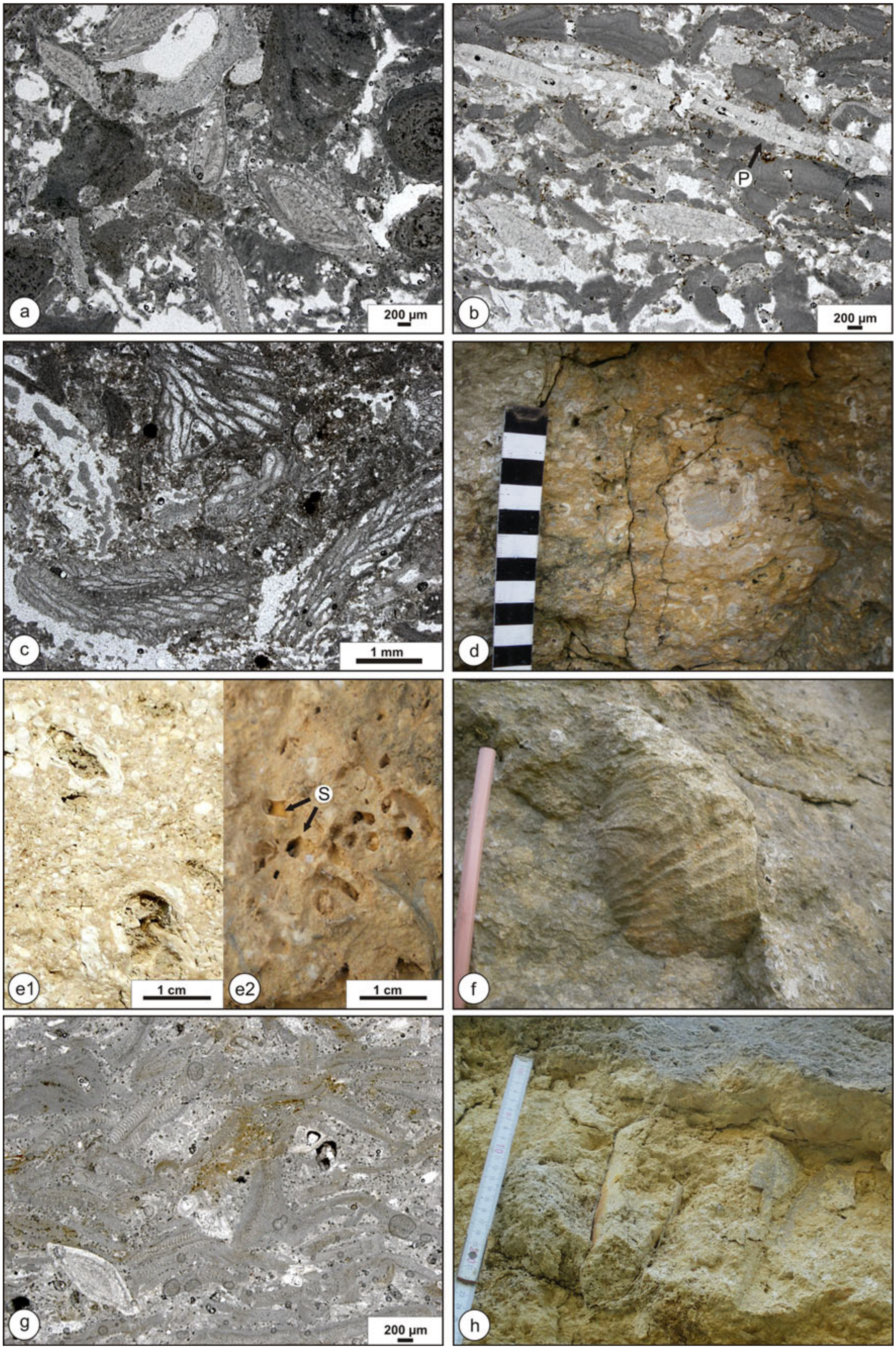
a
200 µm
b
P
200 µm
c
1 mm
d
e1
1 cm
e2
S
1 cm
f
g
200 µm
h

◀ **Fig. 8** *Amphistegina* subfacies. **a** Corallinacean rudstone with common *Amphistegina* (A) and corallinacean debris. **b** Association of *Amphistegina* and *Planostegina* (P) within a corallinacean packstone with common thin encrusting growth forms. **c–d** Bryozoan subfacies. **c** Debris of branched bryozoans within a corallinacean packstone. **d** Corallinacean floatstone with red algae encrusting a celleporiform bryozoan forming a rhodolith. **e1–e2** Coral debris subfacies. **e1** Corallinacean rudstone containing debris of branched *Porites* encrusted by corallinaceans. **e2** Corallinacean rudstone containing debris of *Stylocora*? (S). **f** *Pholadomya* subfacies. Corallinacean floatstone with in situ *Pholadomya alpina* (pencil for scale). **g–h** *Pinna* subfacies. **g** Packstone matrix of a corallinacean rudstone dominated by thin encrusting growth forms. **h** Shell remains and steinkern of in situ *Pinna tetragona* within a corallinacean rudstone

Conesa et al. (2005). The latter authors interpret these limestones as deposits in a high- to moderate-energy environment within or near coral patch reefs. The density of the corals within the limestones in the Mannersdorf sections is rather low and the corals, except *Porites*, which is found in situ, are strongly fragmented. However, these colonies and the associated debris are comparable to the 'coral interval 5' of Riegl and Piller (2000), described from the Fenk quarry. This interval was interpreted as a sparse *Porites*-community on a subtidal soft- or firmground, which formed in a depth range from 3 to 7 m (Riegl and Piller 2000).

Thus, the coral debris subfacies represents deposits in a shallow high- to moderate-energy environment. Similar to the Fenk quarry, the coral patches of Mannersdorf might have formed in less than 10 m water depth.

*Pholadomya subfacies*

The *Pholadomya* subfacies (Fig. 8f) comprises poorly sorted corallinacean rudstones and floatstones. It is dominated by thin encrusting corallinacean growth forms but fruticose growth forms also occur. Branched and celleporiform bryozoans are common, occasionally encrusted by corallinaceans. Foraminifers are represented by biserial textulariids and rotaliids (*Amphistegina*). The facies is characterized by the occurrence of in situ *Pholadomya alpina* (Matheron, 1842) with a total length of 10–15 cm. The associated bivalve fauna consists of *Periglypta miocaenica* and ostreids. Corals are represented by fragmented delicate branched forms. Echinoids occur as isolated spines or highly fragmented coronae. The facies is developed in section II (bed C2) and is associated with the bryozoan subfacies.

Interpretation: The *Pholadomya* subfacies shows similarities to the *Amphistegina* subfacies and the *Pinna* subfacies in microfacies but is characterized by in situ occurrences of *Pholadomya*. Extant Pholadomyidae are deep-burrowing bivalves (Runnegar 1974). Recent *Pholadomya candida* (Sowerby, 1823) burrows in coralline algal sands and seagrass beds (Díaz and Borrero 1995; McIntyre 2010) and was detected in a water depth of 9–25 m (Díaz and Borrero 1995).

A *Pholadomya* facies has already mentioned for Bajocian limestone deposits (Lathuilière 1982). Cretaceous counterparts of the *Pholadomya* subfacies, as described by Lazo (2007) and Armella et al. (2007) are indicative of oxygenated waters of shoreface to inner shelf environments with soft to firm, sandy and bioclastic substrates. The in situ shells of *Pholadomya alpina* (Matheron, 1842) indicate insufficient water energy for exhumation. Recent *Pholadomya* are relatively sensitive to sediment disturbance and indicate deeper water (ca. 40–60 m) with low currents (Schneider 2008). A rather calm sublittoral depositional environment in the aforementioned depth can be postulated for the *Pholadomya* subfacies of Mannersdorf. It indicates the deepest setting in the successions.

*Pinna subfacies*

The *Pinna* subfacies (Fig. 8g, h) comprises poorly sorted marly corallinacean rudstones with packstone matrix, and small lenses of quartz fine-sand and silty clay horizons. The bioclasts have diameters up to 4 mm. The cementation of the limestones varies from very porous to well cemented. The corallinaceans are dominated by encrusting and fruticose growth forms but thin encrusting growth forms can dominate locally. The packstone matrix comprises bioclasts of corallinaceans, mollusc debris, and foraminifers. Foraminifers are dominated by textulariids and rotaliids such as *Amphistegina*; miliolids are generally rare. Local concentrations of *Amphistegina* occur. The mollusc fauna is characterized by *Pinna tetragona*, which commonly occurs in situ. Additional mollusc taxa are *Gigantopecten nodosiformis*, *Aequipecten malvinae* (du Bois de Montpereux, 1831), *Ctena decussata*, *Periglypta miocaenica*, *Glycymeris deshayesi*, *Glans subrudista*, cardiids, and poorly preserved rissoid gastropods. Regular and irregular echinoid remains occur in variable amounts. Celleporiform bryozoans are locally common. Single branches of *Porites* of 2–3 cm length and *Thalassinoides* burrows are typical. The facies is developed in section I (bed 6–9 and the lower part of bed 10) and is associated with the *Acervulina*-rhodolith subfacies and the mollusc subfacies.

Interpretation: The *Pinna* subfacies is similar to the *Amphistegina* subfacies in its microfacies but is characterized by in situ occurrences of the fan mussel *Pinna tetragona*. Modern pinnids are shallow-marine endobyssate suspension-feeders, which are attached by their byssus to the substrate (Richardson et al. 1999). They occur at depths between 0.5 and 60 m within seagrass meadows, half- to mostly embedded in the sediment (Zavodnik et al. 1991; Hofrichter 2002; Rabaoui et al. 2007; Mikkelsen and Bieler 2008). The Recent *Pinna nobilis* (Linnaeus, 1758) is reported in the Mediterranean sea from sandy bottoms in about 3-m water depth, preferentially close to seagrass meadows (Riedl 1983). *Pinna bicolor* (Gmelin, 1791) occurs in South Australia in ca. 7-m water depth (Keough 1984). In sheltered areas, they can also be found in very shallow waters, including intertidal flats (Yonge 1953; Stanley 1970; Butler et al. 1993). The lucinid bivalve *Ctena decussata*, which bears chemosymbiotic bacteria, also prefers shallow seagrass meadows (Taylor and Glover 2000). At Mannersdorf, this bivalve is restricted to the *Pinna* subfacies. Modern counterparts of *Codakia* also bear chemosymbiotic bacteria and settle preferentially within seagrass meadows (Schweimanns and Felbeck 1985) but *Porites* can develop small patches within seagrass environments (Riegl and Piller 2000; Wulff 2008). Quartz fine-sand lenses and clay horizons might go back to the baffling of seagrasses (Tucker and Wright 1990).

Hence, the *Pinna* subfacies has developed in a very shallow environment (<10 m) in moderately agitated water within seagrass meadows. Low-oxygen conditions in the sediment might be indicated by the abundance of lucinids (Emery and Hulsemann 1962). Such conditions can be caused by decomposition of large quantities of organic material (Eyre and Ferguson 2002), mostly seagrass.

### Rhodolith facies

The rhodolith facies (Fig. 9a, b) is characterized by a poorly cemented corallinacean rudstone dominated by densely packed, mostly spheroidal to ellipsoidal rhodoliths, cm to dm in size, with a warty surface. Interspaces between rhodoliths are filled with clasts of corallinaceans with fruticose and encrusting growth forms. *Acervulina* often encrusts corallinaceans. Other components are formed by molluscs (ostreids) and encrusting bryozoans. Foraminifers are represented by rotaliids (*Amphistegina*) and miliolids (*Triloculina*). The facies is developed in section II (bed C7). It is associated with the coral debris subfacies.

Interpretation: The facies is similar to the rhodolith pavement facies of Dullo (1983) near St. Margarethen. According to Steneck (1986), rhodolith pavements are formed by unattached coralline algae including rhodoliths. A paleoenvironmental interpretation, based only on rhodolith morphologies, is difficult due to the complex interplay between water movement, transport, substrate type, and bioturbation (Steller and Foster 1995; Marrack 1999; Foster 2001; Bassi et al. 2009). As a rule of thumb, low-energy environments are characterized by open-branched rhodoliths, while high water agitation is reflected by massive, densely branched or even laminar rhodolith growth forms (Bosence 1979, 1983, 1991; Bosence and Pedley 1982; Studencki 1988).

The shapes of rhodoliths in Mannersdorf fit well with the mainly spheroidal IG-Type of Bassi et al. (2006), which is interpreted to be indicative of moderate to high water turbulence and low substrate stability. However, similar sediments of the Latium-Abruzzi Platform show no indication of high current regimes. These limestones rather indicate low sedimentation rates and biogenically induced periodic turning (Brandano and Piller 2010). This may be induced by crustaceans or foraging fish (Marrack 1999). Hence the rhodolith facies seems to reflect a very shallow water depth with hydrodynamics similar to the *Acervulina*-rhodolith subfacies. This facies is similar to Recent rhodolith accumulations described from the Gulf of California, Ryukyu Islands, and Lord Howe Island (Bassi and Nebelsick 2010 and further references therein). Rhodolith belts in the modern Red Sea are adjacent to seagrass meadows and coral zones (cf. Piller and Rasser 1996).

## Facies zonations

Combining the results of field observations and microfacies analysis, a facies zonation for the Mannersdorf locality can be developed for the subtypes of the bioclastic corallinacean facies and for the rhodolith facies.

In very shallow settings (<10 m), the *Pinna* subfacies is developed, which represents seagrass meadows baffling sand and mud under moderate water energy. The coral debris subfacies and the adjacent rhodolith facies developed in a similar water depth with higher water energy. The *Acervulina*-rhodolith subfacies, intercalated within gravels or terminating the latter, indicates slight deepening due to marine transgression. The *Acervulina*-rhodolith subfacies is adjoining to the mollusc subfacies, which represents a deeper environment (ca. 20–30 m) with moderate water energy. It is associated with the *Amphistegina* subfacies, which again mirrors deeper water with a range of 20–30 m. Transitions from the mollusc subfacies to the bryozoan subfacies go along with deeper water (below 30 m) and lower energy levels. The deepest setting is represented by the *Pholadomya* subfacies, indicating a water depth of ca. 40–60 m with low water energy. The remaining facies types of Mannersdorf belong to a separate system. The basal breccia facies and the cross-bedded gravel facies represent high-energy environments with a few meters of water depth. While the basal breccia facies represents coastal scree onlapping on a cliff, the cross-bedded gravel facies shows characteristics of a prograding delta.

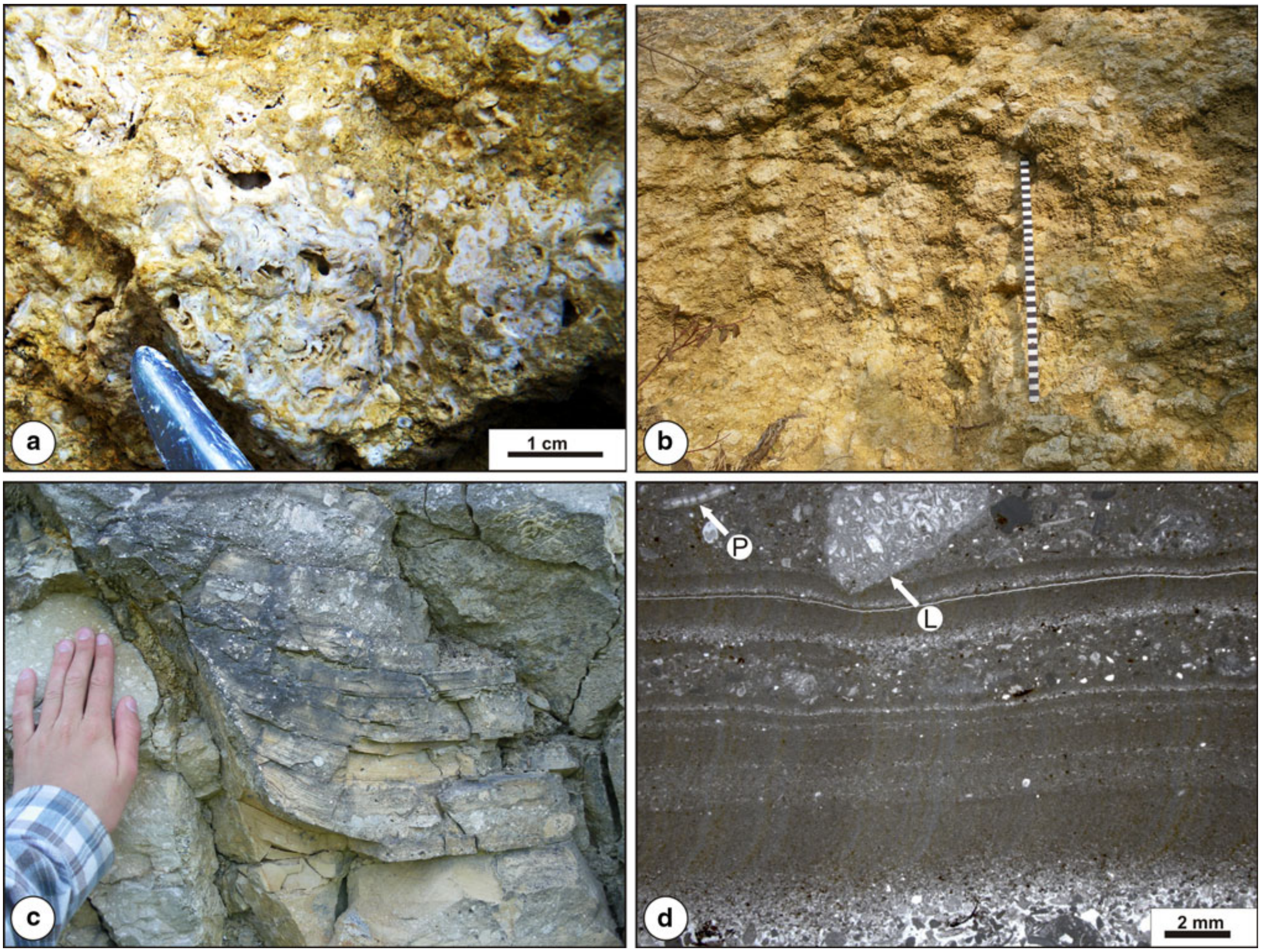


**Fig. 9** Rhodolith facies. **a** Ellipsoidal rhodoliths with warty surfaces. **b** Accumulations of densely packed spheroidal to ellipsoidal rhodoliths. **c–d** Neptunian dyke. **c** Fissure (hand for scale) filled with well-cemented thin mm-layered marly pack-, wacke-, and mudstone. **d** Reworked clast (L) forming a load cast on laminated layers below, *Planostegina* (P)

## Facies succession and synsedimentary tectonics

Deposition of the lowermost sediments started during rising relative sea-level with the development of dolostone breccias and river-transported gravels (Fig. 5a). A relative sea-level rise is indicated by onlapping of the dolostone breccia onto the dolostone. The limestone bed intercalated within the gravels may reflect a distinct transgressive pulse. It is again overlain by gravels of a prograding river delta. The gravel body is terminated by corallinacean limestones (Fig. 10a), which indicate a strong relative sea-level rise by development of the deepest sediments. They are characterized by the common occurrence of *Pholadomya alpina*, which prefers calmer, deeper habitats. Falling relative sea-level (Fig. 5b) is indicated by a shallowing-upward trend expressed in facies types deposited in relatively shallower-marine settings. Onsetting tectonic movement divided the area into two independent blocks (Fig. 10b). The tectonic movements (Fig. 6) verify a normal-fault (southwestern block as hanging wall) with dextral strike-slip tectonics due to ENE–WSW and N–S-trending extensions. The fault zone shows a normal fault reactivated as a dextral strike-slip fault. A flexure enabled the onlap of sediments. This happened during a relative sea-level fall (indicated by deposition of the *Acervulina*-rhodolith facies in section I). At the same time, a relative sea-level fall led to erosion or non-deposition on the northeastern block (footwall) indicated by an unconformity in section II. The rapid facies change from the bryozoan subfacies to the coral debris subfacies (bed C5–C6) also indicates a break in sedimentation. On the southwestern block, sedimentation kept up with subsidence and gradually changed from deeper to shallower facies types. With relative rise of sea-level, shallow-water carbonates were formed on both blocks (Fig. 10c), represented by the coral debris subfacies on the northeastern block and the *Pinna* subfacies on the southwestern block. During tectonic activity, also the jointset in section II was formed, which was filled with fine-grained

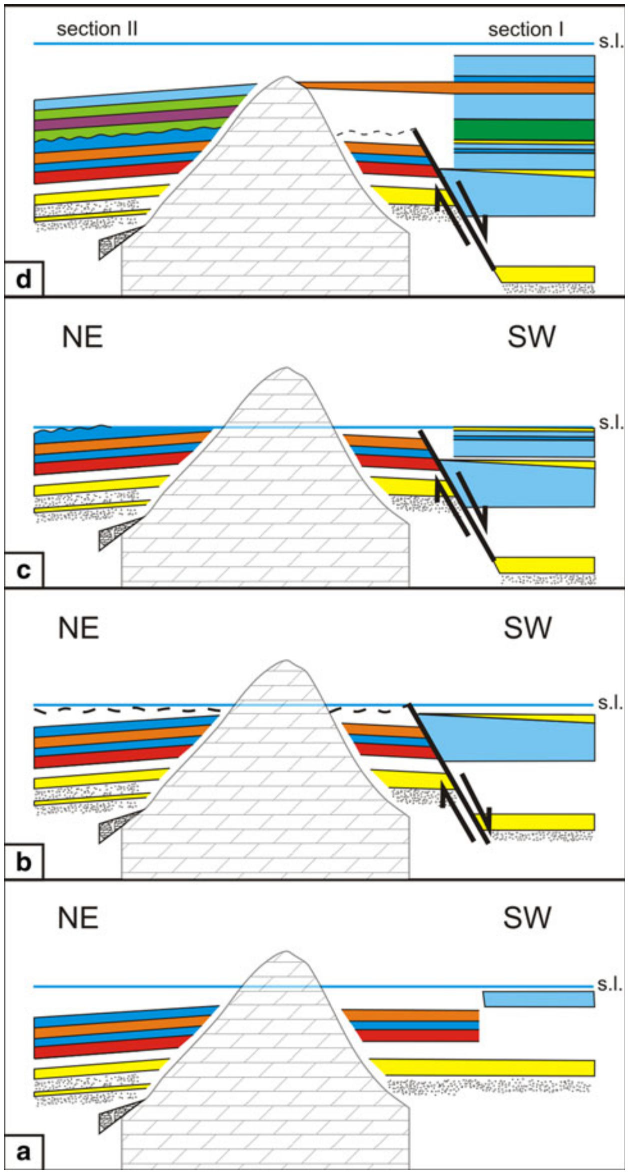


**Fig. 10** Depositional model illustrating tectonic activity. *Arrows* show displacement directions during thrusting. Facies types are highlighted with *colors* (cf. Fig. 3). Starting with undisturbed sedimentation (**a**), a phase of synsedimentary tectonics (**b**–**c**) follows. The last stage is characterized by flooding and undisturbed sedimentation (**d**)

sediments and therefore acted as a neptunian dyke (Fig. 5c). With ongoing relative sea-level rise (Fig. 10d), the *Amphistegina* subfacies developed on both tectonic blocks, onlapping onto the dolostone in a water depth of ca. 20–30 m. Its deposition indicates tectonic inactivity and burial of the fault.

In comparison to the Fenk quarry at the southwestern edge of the Leitha Mountains, which reflects environments similar to the modern Red Sea and the Arabian Gulf (Riegl and Piller 2000), the poor coral fauna and some mollusc assemblages have more similarities to modern environments (such as seagrass meadows) represented in the Florida Keys (e.g., Mikkelsen and Bieler 2008).

## Conclusions

The Leitha Limestones of the Mannersdorf quarries (Lower Austria) preserve records of pre-, syn-, and post-tectonical phases of carbonate deposition on a Badenian shallow-water carbonate platform in the Vienna Basin with a transition from a siliciclastic to a carbonate depositional environment. The pre-tectonical phase is represented by the flooding of a Mesozoic dolostone during a marine transgression with the development of a coastal slope scree and subsequent progradation of a Gilbert-type fan delta. Facies analyses of the overlying very heterogeneous corallinacean limestones reveals a continuous water depth increase by the vertical transition from the *Acervulina*-rhodolith subfacies to the bryozoan subfacies and the *Pholadomya* subfacies. Subsequently, a fault divided the study area into a northern and a southern tectonic block. Paleostress analyses verify a normal fault reactivated as a dextral strike-slip fault. This syn-tectonical phase corresponds with a relative sea-level fall. While the northern block was partly eroded, the southern block indicates tectonical movements with onlap of limestones on a tectonic-caused flexure and development of seagrass meadows (*Pinna* subfacies). A post-tectonic phase with renewed marine transgression and onlapping of deeper water carbonates (*Amphistegina* subfacies) on the dolostone is indicated by burial of the fault and development of a neptunian dyke. A facies model comprising corallinacean limestones of both blocks combines the results of field observations and microfacies analysis and illustrates transitions from shallow-water carbonates such as the *Pinna* subfacies to the deepest observed carbonates, represented by the *Pholadomya* subfacies.

**Acknowledgments** This paper was financed by the “NAWI Graz Advanced School of Science” (GASS). Field work was kindly encouraged by the Lafarge-Perlmooser AG; special thanks go to the raw material- and quarry manager Dipl.-Ing. Ralf Baehr-Mörsen for his support. Many thanks go to Dr. Markus Reuter (University of Graz), Dr. Ulrike Exner (University of Vienna), and Dr. Harald Fritz (University of Graz) for constructive discussions. For determination of bivalve remains, we would like to thank Dr. Oleg Mandic (Natural History Museum Vienna), for determination of echinoid remains Dr. Andreas Kroh (Natural History Museum Vienna). Thanks also go to Hans Schwengersbauer (Mannersdorf museum of local history) for reports of decades of mining activity. Finally, we thank Dr. Steven J. Weiss (University of Graz) for improving the English of the manuscript. The manuscript benefited from the constructive comments of the reviewers Dr. Martin Zuschin (University of Vienna) and Dr. James Nebelsick (University of Tübingen), and from the editorial advice of Dr. Franz Theodor Fürsich (University of Erlangen-Nürnberg).

## References

Adams GC, Lee DE, Rosen BR (1990) Conflicting isotopic and biotic evidence for tropical sea-surface temperatures during the Tertiary. Palaeogeogr Palaeoclimatol Palaeoecol 77:289–313

Adey WH (1986) Coralline algae as indicators of sea-level. In: Van de Plassche O (ed) Sea-level research: a manual for the collection and evaluation of data. Geo Books, Norwich, pp 229–280

Armella C, Cabaleri N, Leanza HA (2007) Tidally dominated, rimmed-shelf facies of the Picún Leufú Formation (Jurassic/Cretaceous boundary) in southwest Gondwana, Neuquén Basin, Argentina. Cret Res 28:961–979

Barbera C, Simone L, Carannante G (1978) Depositi circalittorali di piattaforma aperta nel Miocene Campano. Analisi sedimentologica e paleoecologica. Boll Soc Geol It 97:821–834

Baskar S, Baskar R, Natuschka L, Kaushik A, Theophilus PK (2008) Precipitation of iron in microbial mats of the spring waters of Borra Caves, Vishakapatnam, India: some geomicrobiological aspects. Environ Geol 56:237–243

Bassi D, Humblet M (2011) Recent ichnocoenosis in deep-water macroids, Ryukyu Islands, Japan. Palaios 26:232–238

Bassi D, Nebelsick JH (2010) Components, facies and ramps: Redefining Upper Oligocene shallow-water carbonates using coralline red algae and larger foraminifera (Venetian area, northeast Italy). Palaeogeogr Palaeoclimatol Palaeoecol 295: 258–280

Bassi D, Carannante G, Monleau C, Murru M, Simone L, Toscano F (2006) Rhodalgal/bryomol assemblages in temperate type carbonate, channelized depositional systems: the Early Miocene of the Sarcidano area (Sardinia, Italy). In: Pedley HM, Carannante G (eds) Cool-water carbonates. Depositional systems and palaeoenvironmental controls. Geol Soc Spec Publ 255:35–52

Bassi D, Nebelsick JH, Checconi A, Hohenegger J, Iryu Y (2009) Present-day and fossil rhodolith pavements compared: their potential for analysing shallow-water carbonate deposits. Sediment Geol 214:74–84

Basso DM, Vrsaljko D, Grgasović T (2008) The coralline flora of a Miocene maërl: the Croatian "Litavac". Geol Croatica 61(2–3):333–340

Betzler C, Brachert TC, Kroon D (1995) Role of climate for partial drowning of the Queensland Plateau carbonate platform (northeastern Australia). Mar Geol 123:11–32

Bosellini F, Papazzoni C (2003) Paleoecological significance of coral-encrusting foraminifera associations: a case-study from the Upper Eocene of northern Italy. Acta Palaeont Polon 48:279–292

Bosence DWJ (1976) Ecological studies on two unattached coralline algae from western Ireland. Palaeontology 19:365–395

Bosence DWJ (1979) Live and dead faunas from coralline algal gravels, Co. Galway. Palaeontology 22:449–478

Bosence DWJ (1983) Coralline algae from the Miocene of Malta. Palaeontology 26:147–173

Bosence DWJ (1991) Coralline algae: mineralization, taxonomy, and palaeoecology. In: Riding R (ed) Calcareous algae and stromatolites. Springer, Berlin Heidelberg New York, pp 98–113

Bosence DWJ, Pedley HM (1979) Palaeoecology of a Miocene coralline algal bioherm, Malta. Bull Centr Rech Expl Prod Elf-Aquitaine 3:463–470

Bosence DWJ, Pedley HM (1982) Sedimentology and palaeoecology of a Miocene coralline algal biostrome from the Maltese Islands. Palaeogeogr Palaeoclimatol Palaeoecol 38:9–43

Brandano M, Piller WE (2010) Coralline algae, oysters and echinoids—a liaison in rhodolith formation from the Burdigalian of the Latium-Abruzzi Platform (Italy). In: Mutti M, Piller WE, Betzler C (eds) Carbonate systems during the Oligocene-Miocene climatic transition. Int Assoc Sedimentol Spec Publ 42:149–164

Butler AJ, Vicente N, De Gaulejac B (1993) Ecology of the pterioid bivalves *Pinna bicolor* Gmelin and *Pinna nobilis* L. Mar Life 3:37–45

Cabioch L (1968) Contribution à la connaissance des peuplements benthiques de la Manche occidentale. Cah Biol Mar 9:493–720

Conesa GAR, Favre E, Münch P, Dalmasso H, Chaix C (2005) Proceedings of the Ocean Drilling Program (Northeast Australia, ODP Leg 194, Sites 1196 and 1199). In: Anselmetti F, Isern AR, Blum P, Betzler C (eds) Proc ODP Sci Results 194:1–38

Decker K (1996) Miocene tectonics at the Alpine-Carpathian junction and the evolution of the Vienna basin, Mitt. Ges Geol Bergbaustud Österr 41:33–44

Decker K, Peresson H (1996) Tertiary kinematics in the Alpine-Carpathian-Pannonian system: links between thrusting, transform faulting and crustal extension. In: Wessely G, Liebl W (eds) Oil and gas in Alpidic thrusts and basins of Central and Eastern Europe. Eur Assoc Geosci Eng Spec Publ 5:69–77

Delvaux D, Sperner B (2003) Stress tensor inversion from fault kinematic indicators and focal mechanism data: the TENSOR program. In: Nieuwland D (ed) New insights into structural interpretation and modelling: Geol Soc Lond Spec Publ 212:75–100

Díaz JM, Borrero FJ (1995) On the occurrence of *Pholadomya candida* Sowerby, 1823 (Bivalvia: Anomalodesmata) on the Caribbean coast of Colombia. J Moll Stud 61:407–408

Dullo WC (1983) Diagenesis of fossils of the Miocene Leitha Limestone of the Paratethys, Austria: An example for faunal modifications due to changing diagenetic environments. Facies 8:1–112

Dunham RJ (1962) Classification of carbonate rocks according to their depositional texture. In: Ham WE (ed) Classification of carbonate rocks–a symposium. Am Assoc Petrol Geol Mem 1:108–121

Embry AF, Klovan JE (1971) A late Devonian reef tract on Northeastern Banks Island, NWT. Can Petrol Geol Bull 19:730–781

Emery KO, Hulsemann J (1962) The relationship of sediments, life, and water in a marine basin. Deep Sea Res 8:165–180

Eyre BD, Ferguson AJP (2002) Comparison of carbon production and decomposition, benthic nutrient fluxes and denitrification in seagrass, phytoplankton, benthic microalgal and macroalgal dominated warm temperate Australian lagoons. Mar Ecol Prog Ser 229:43–59

Fencl M (2005) Sedimentologie der klastischen Miozän-Abfolgen in Mannersdorf am Leithagebirge (Niederösterreich). Unpubl. Diploma Thesis, Univ. Wien

Fodor L (1995) From transpression to transtension: Oligocene-Miocene structural evolution of the Vienna basin and the East Alpine-Western Carpathian junction. Tectonophysics 242:151–182

Foster MS (2001) Rhodoliths: between rocks and soft places. J Phycol 87:659–667

Freiwald A (1994) Sedimentological and biological aspects in the formation of branched rhodoliths in northern Norway. Beitr Paläontol Österr 20:7–19

Freiwald A, Henrich R, Schäfer P, Willkomm H (1991) The significance of high-boreal to subarctic maerl deposits in northern Norway to reconstruct Holocene climatic changes and sea level oscillations. Facies 25:315–340

Fuchs T (1894) Ueber abgerollte Blöcke von Nulliporen-Kalk im Nulliporen-Kalk von Kaisersteinbruch. Z Deutsch Geol Ges 46:126–130

Fujita K, Osawa Y, Kayanne H, Ide Y, Yamano H (2009) Distribution and sediment production of large benthic foraminifers on reef flats of the Majuro Atoll, Marshall Islands. Coral Reefs 28:29–45

García-García F, Fernández J, Viseras C, Soria JM (2006) High frequency cyclicity in a vertical alternation of Gilbert-type deltas and carbonate bioconstructions in the late Tortonian, Tabernas Basin, southern Spain. Sediment Geol 192:123–139

Harzhauser M, Piller WE (2004) The Early Sarmatian–hidden seesaw changes. Cour Forschinst Senckenberg 246:89–111

Harzhauser M, Piller WE (2007) Benchmark data of a changing sea–Palaeogeography, palaeobiogeography and events in the Central Paratethys during the Miocene. Palaeogeogr Palaeoclimatol Palaeoecol 253:8–31

Harzhauser M, Piller WE (2010) Molluscs as a major part of subtropical shallow-water carbonate production—an example from a Middle Miocene oolite shoal (Upper Serravallian, Austria). Spec Publ Int Ass Sed 42:185–200

Häusler H, Figdor H, Hammerl C, Kohlbeck F, Lenhardt W, Schuster R (2010) Geologische Karte der Republik Österreich 1:50.000, Erläuterungen zu Blatt 78 RUST. Geologische Bundesanstalt, Wien

Herrmann P (1973) Geologie der Umgebung des östlichen Leithagebirges (Burgenland). Mitt Ges Geol Bergbaustud Österr 1973:165–189

Herrmann P, Pascher GA, Pistotnik J (1993) Geologische Karte der Republik Österreich 1.50.000, Blatt 78 Rust. Geol Bundesanstalt, Wien

Hofrichter R (2002) Das Mittelmeer–Fauna, Flora, Ökologie, Band I: Allgemeiner Teil. Spektrum Akademischer Verlag, Heidelberg

Hohenegger J, Wagreich M (2011) Time calibration of sedimentary sections based on isolation cycles using combined cross-correlation: dating the gone Badenian stratotype (Middle Miocene, Paratethys, Vienna Basin, Austria) as an example. Int J Earth Sci (Geol Rundsch). doi:10.1007/s00531-011-0658-y

Hohenegger J, Yordanova E, Hatta A (2000) Remarks on West Pacific Nummulitidae (Foraminifera). J Foram Res 30:3–28

Hölzel M, Wagreich M, Faber R, Strauss P (2008) Regional subsidence analysis in the Vienna Basin (Austria). Austrian J Earth Sci 101:88–98

Hottinger L (1983) Neritic macroid genesis, an ecological approach. In: Peryt TM (ed) Coated grains. Springer, Berlin Heidelberg New York, pp 37–55

Iryu Y, Nakamori T, Matsuda S, Abe O (1995) Distribution of marine organisms and its geological significance in the modern reef complex of the Ryukyu Islands. Sediment Geol 99:243–258

James DW, Foster MS, O'Sullivan J (2006) Bryoliths (Bryozoa) in the Gulf of California. Pac Sci 60:117–124

Jannsen R, Zuschin M, Baal C (2011) Gastropods and their habitats from the northern Red Sea (Egypt: Safaga). Part 2: Caenogastropoda: Sorbeoconcha and Littorinimorpha. Ann Naturhist Mus Wien 113(A):373–509

Keegan BF (1974) The macrofauna of maerl substrates on the west coast of Ireland. Cah Biol Mar 15:513–530

Keferstein C (1828) Beobachtungen und Ansichten über die geognostischen Verhältnisse der nördlichen Kalk-Alpenkette in Österreich-Bayern. Teutschland geognostisch-geologisch dargestellt 5(3):1–425

Keough MJ (1984) Dynamics of the epifauna of the bivalve *Pinna bicolor*: interactions among recruitment, predation, and competition. Ecology 65:677–688

Klimcouk AB (2007) Hypogene speleogenesis: hydrogeological and morphogenetic perspective. Nat Cave Karst Res Inst Spec Pap 1:1–102

Konhauser KO, Ferris FG (1996) Diversity of iron and silica precipitation by microbial mats in hydrothermal waters, Iceland: Implications for Precambrian iron formations. Geology 24:323–326

Kröll AW, Wessely G (1993) Strukturkarte Basis der tertiären Beckenfüllung. Geologische Themenkarte der Republik Österreich. Wiener Becken und angrenzende Gebiete 1: 200.000. Geol Surv Austria, Vienna

Lankreijer A, Kovac M, Cloetingh S, Pitonak P, Hloska M, Biermann C (1995) Quantitative subsidence analysis and forward modelling of the Vienna and Danube basins: thin-skinned versus thick-skinned extension. Tectonophysics 252:433–451

Larsen AR (1976) Studies of recent *Amphistegina*, taxonomy and some ecological aspects. Israel J Earth Sci 25:1–26

Laskarev VN (1924) Sur les equivalentes du Sarmatien supérieur en Serbie. Zborník Cvijic, pp 73–85

Lathuilière B (1982) Bioconstructions bajociennes à madréporaires et faciès associés dans l'Île Crémieu (Jura du Sud; France). Geobios 15:491–504

Lazo DG (2007) The bivalve *Pholadomya gigantea* in the Early Cretaceous of Argentina: Taxonomy, taphonomy, and paleogeographic implications. Acta Palaeont Polon 52:375–390

Ludbrook NH, Gowlett-Holmes KL (1989) Chitons, gastropods, and bivalves. In: Shepherd SA, Thomas IM (eds) Marine invertebrates of southern Australia, Part II. Government Printer, South Australia, Adelaide, pp 504–724

Marrack EC (1999) The relationship between water motion and living rhodolith beds in the southwestern Gulf of California, Mexico. Palaios 14:159–171

McIntyre AD (2010) Life in the world's oceans. Diversity, distribution, and abundance. Blackwell, Oxford

McPherson JG, Shanmugam G, Moiola RJ (1987) Fan-deltas and braid deltas: varieties of coarse-grained deltas. Geol Soc Am Bull 99:331–340

Mikkelsen PM, Bieler R (2008) Seashells of southern Florida: living marine mollusks of the Florida Keys and adjacent regions: Bivalves. Princeton University Press, Princeton

Papp A, Cicha I (1978) Definition der Zeiteinheit M—Badenien. In: Papp A, Cicha I, Seneš J, Steininger FF (eds) M4—Badenien (Moravien, Wielicien, Kosovien). Chronostratigraphie und Neostratotypen. Miozän der Zentralen Paratethys. Slowakische Akademie der Wissenschaften, Bratislava, pp 47–48

Perrin C (1994) Morphology of encrusting and free living acervulinid foraminifera: *Acervulina*, *Gypsina*, and *Solenomeris*. Palaeontology 37:425–458

Piller WE, Rasser M (1996) Rhodolith formation induced by reef erosion in the Red Sea, Egypt. Coral Reefs 15:191–198

Piller WE, Kleemann K, Friebe JG (1991) Miocene reefs and related facies in Eastern Austria. In: Excursion B4. Guidebook of the VI international symposium on Fossil Cnidaria including Archaeocyatha and Porifera. International Association for the Study of Fossil Cnidaria and Porifera, Münster

Piller WE, Harzhauser M, Mandic O (2007) Miocene Central Paratethys stratigraphy—current status and future directions. Stratigraphy 4:151–168

Plan L, Pavuza R, Seemann R (2006) Der Nasse Schacht bei Mannersdorf am Leithagebirge, NÖ (2911/21)—eine thermal beeinflusste Höhle am Ostrand des Wiener Beckens. Die Höhle 57:30–46

Postma G (1990) Depositional architecture and facies of river and fan deltas: a synthesis. Spec Publ Int Ass Sediment 10:13–27

Prager EJ, Ginsburg RN (1989) Carbonate nodule growth on Florida's outer shelf and its implications for fossil interpretations. Palaios 4:310–317

Rabaoui L, Tlig Zouari S, Katsanevakis S, Kalthoum O, Hassine B (2007) Comparison of absolute and relative growth patterns among five *Pinna nobilis* populations along the Tunisian coastline: an information theory approach. Mar Biol 152:537–548

Rasser M (2000) Coralline red algal limestones of the Late Eocene Alpine Foreland Basin in Upper Austria: components analysis, facies and paleoecology. Facies 42:59–92

Rasser M, Piller WE (1997) Depth distribution of calcareous encrusting associations in the northern Red Sea (Safaga, Egypt) and their geological implications. Proc 8th Int Coral Reef Symp 1:743–748

Ratschbacher L, Behrmann JH, Pahr A (1990) Penninic windows at the eastern end of the Alps and their relation to the intra-Carpathian basins. Tectonophysics 172:91–105

Ratschbacher L, Frisch W, Linzer HG, Merle O (1991) Lateral extrusion in the Eastern Alps. Tectonics 10:257–271

Reid RP, Macintyre IG (1988) Foraminiferal-algal nodules from the Eastern Caribbean: growth history and implications on the value of nodules as paleoenvironmental indicators. Palaios 3:424–435

Renema W (2006) Large benthic foraminifera from the deep photic zone of a mixed siliciclastic-carbonate shelf off East Kalimantan, Indonesia. Mar Micropaleont 58:73–82

Richardson CA, Kennedy H, Duarte CM, Kennedy DP, Proud SV (1999) Age and growth of the fan mussel *Pinna nobilis* from south-east Spanish Mediterranean seagrass (*Posidonia oceanica*) meadows. Mar Biol 133:205–212

Rider J, Enrico R (1979) Structural and functional adaptations of mobile anascan ectoproct colonies (ectoproctaliths). In: Larwood GP, Abbott MB (eds) Advances in bryozoology. Academic Press, New York, pp 297–319

Riedl R (1983) Fauna und Flora des Mittelmeeres. Verlag Paul Parey, Hamburg

Riegl B, Piller WE (2000) Biostromal coral facies—a Miocene example from the Leitha Limestone (Austria) and its actualistic interpretation. Palaios 15:399–413

Rohatsch A (1997) Gesteinskunde in der Denkmalpflege unter besonderer Berücksichtigung der jungtertiären Naturwerksteine von Wien, Niederösterreich und dem Burgenland. Unpubl. Habilitation-Thesis, Wien

Rohatsch A (2008) Die Baugesteine des Wiener Stephansdomes. J Alpine Geol (Mitt Ges Geol Bergbaustud Österr) 49:197–200

Royden LH (1985) The Vienna Basin: a thin-skinned pull-apart basin. In: Biddle KT, Christie-Blick N (eds) Strike-Slip deformation, basin formation, and sedimentation. SEPM Spec Publ 37:319–338

Runnegar B (1974) Evolutionary history of the Bivalve subclass Anomalodesmata. J Paleont 48:904–939

Sarà G (1969) Research on coralligenous formations: problems and perspectives. Pubbl Staz Zool di Napoli 37:124–134

Schaffer FX (1908) Geologischer Führer für Exkursionen im Inneralpinen Wienerbecken II. Teil. Sammlung geologischer Führer 13, Berlin (Borntraeger)

Schlanger SO, Johnson CJ (1969) Algal banks near La Paz, Baja California—Modern analogues of source areas of transported shallow-water fossils in pre-alpine flysch deposits. Palaeogeogr Palaeoclimatol Palaeoecol 6:141–157

Schmid HP, Harzhauser M, Kroh A (2001) Hypoxic events on a Middle Miocene carbonate platform of the Central Paratethys (Austria, Badenian, 14 Ma). Ann Naturhist Mus Wien 102(A): 1–50

Schneider S (2008) The bivalve fauna from the Ortenburg Marine Sands in the well-core “Straß” (Early Miocene; SE Germany)—taxonomy, stratigraphy, paleoecology, and paleogeography. Paläont Z 82:402–417

Schweimanns M, Felbeck H (1985) Significance of the occurrence of chemoautotrophic bacterial endosymbionts in lucinid clams from Bermuda. Mar Ecol Prog Ser 24:113–120

Seifert P (1992) Palinspastic reconstruction of the eastern-most Alps between upper Eocene and Miocene. Geol Carpath 43:327–331

Sohs F (1963) Das Neogen am Westrande des Leithagebirges (zwischen Hornstein und Sommerein). Unpubl. PhD-thesis, Wien

Stanley SM (1970) Relation of shell form to life habits of the Bivalvia (Mollusca). Geol Soc Am Mem 125:1–296

Steininger FF, Rögl F (1984) Paleogeography and palinspastic reconstruction of the Neogene of the Mediterranean and Paratethys. SEPM Spec Publ 17:659–668

Steller DL, Foster MS (1995) Environmental factors influencing distribution and morphology of rhodoliths in Bahía Concepción, B.C.S., México. J Exp Mar Biol Ecol 194:201–212

Steneck RS (1986) The ecology of coralline algal crusts: convergent patterns and adaptative strategies. Annu Rev Ecol Syst 17:273–303

Strauss P, Harzhauser M, Hinsch R, Wagreich M (2006) Sequence stratigraphy in a classic pull-apart basin (Neogene, Vienna Basin). A 3D seismic based integrated approach. Geol Carpath 57:185–197

Studencki W (1988) Facies and sedimentary environment of the Pinczow limestones (Middle Miocene; Holy cross mountains, central Poland). Facies 18:1–26

Studencki W (1999) Red-algal limestone in the Middle Miocene of the Carpathian Foredeep in Poland: facies variability and palaeoclimatic implications. Geol Quat 43:395–404

Taylor JD, Glover EA (2000) Functional anatomy, chemosymbiosis and evolution of the Lucinidae. In: Harper, EM, Taylor JD, Crame JA (eds) The evolutionary biology of the Bivalvia. Spec Publ Geol Soc Lond 177:207–225

Tollmann A (1964) Exkursion II/6, Semmering-Grauwackenzone. Mitt Geol Ges Wien 57:193–203

Tollmann A (1976) Analyse des klassischen nordalpinen Mesozoikums. Deuticke, Wien

Toscano F, Sorgente B (2002) Rhodalgal-bryomol temperate carbonates from the Apulian Shelf (southwestern Italy), relict and modern deposits on a current dominated shelf. Facies 46:103–118

Toscano F, Vigliotti M, Simone L (2006) Variety of coralline algal deposits (rhodalgal facies) from the Bays of Naples and Pozzuoli (northern Tyrrhenian Sea, Italy). In: Pedley HM, Carannante G (eds) Cool-water carbonates: Depositional systems and palaeoenvironmental controls. Geol Soc Lond Spec Publ 255:85–94

Tucker ME, Wright VP (1990) Carbonate sedimentology. Blackwell, Oxford

Varrone D, D’Atri A (2007) Acervulinid macroid and rhodolith facies in the Eocene Nummulitic Limestone of the Dauphinois Domain (Maritime Alps, Liguria, Italy). Swiss J Geosci 100:503–515

Wagreich M, Schmid HP (2002) Backstripping dip-slip fault histories: apparent slip rates for the Miocene of the Vienna Basin. Terra Nova 14:163–168

Wentworth CK (1922) A scale of grade and class terms for clastic sediments. J Geol 30:377–392

Wessely G (1983) Zur Geologie und Hydrodynamik im südlichen Wiener Becken und seiner Randzone. Mitt Geol Ges Wien 76:27–68

Wessely G (1988) Structure and development of the Vienna Basin in Austria. Am Assoc Petro Geol Mem 45:333–346

Wessely G (2006) Geologie der Österreichischen Bundesländer—Niederösterreich. Geologische Bundesanstalt, Wien

Woelkerling WJ, Irvine LM, Harvey AS (1993) Growth-forms in non-geniculate coralline red algae (Corallinales, Rhodophyta). Aust Syst Bot 6:277–293

Wulff JL (2008) Collaboration among sponge species increases sponge diversity and abundance in a seagrass meadow. Mar Ecol 29:193–204

Yonge CM (1953) Form and habit in *Pinna carnea* Gmelin. Phil Trans R Soc Lond, Ser B Biol Sci 237:335–374

Yonge CM (1971) On the functional morphology and adaptive radiation in the bivalve superfamily Saxicavacea (*Hiatella* (= *Saxicava*), *Saxicavella*, *Panomya*, *Panope*, *Cyrtodaria*). Malacologia 11:1–44

Zavodnik D, Hrs-Brenko M, Legac M (1991) Synopsis on the fan shell *Pinna nobilis* L. in the eastern Adriatic Sea. In: Boudouresque CF, Avon M, Gravez V (eds) Les espèces marines à protéger en Méditerranée. GIS Posidonie Publ., Marseille, pp 169–178

Zuschin M, Hohenegger J (1998) Subtropical coral-reef associated sedimentary facies characterized by molluscs (Northern Bay of Safaga, Red Sea, Egypt). Facies 38:229–254

Zuschin M, Janssen R, Baal C (2009) Gastropods and their habitats from the northern Red Sea (Egypt: Safaga). Part 1: Patellogastropoda, Vetigastropoda and Cycloneritimorpha. Ann Naturhist Mus Wien 111(A):73–158